



# PACIFIC EARTHQUAKE ENGINEERING RESEARCH CENTER

## **Fragilities for Precarious Rocks at Yucca Mountain**

**Matthew D. Purvance  
Rasool Anooshehpour  
James N. Brune**

Nevada Seismological Laboratory  
University of Nevada, Reno  
Reno, Nevada

#### Disclaimer

The opinions, findings, and conclusions or recommendations expressed in this publication are those of the author(s) and do not necessarily reflect the views of the study sponsor(s) or the Pacific Earthquake Engineering Research Center.

# **Fragilities for Precarious Rocks at Yucca Mountain**

**Matthew D. Purvance  
Rasool Anoooshehpour  
James N. Brune**

Nevada Seismological Laboratory  
University of Nevada, Reno  
Reno, Nevada

PEER Report 2012/06  
Pacific Earthquake Engineering Research Center  
Headquarters at the University of California

December 2012



## ABSTRACT

Geomorphic features easily damaged by ground shaking can be used to constrain unexceeded ground motions during the feature residence times. Such features, in the form of precariously balanced rocks and fragile rock stacks, exist on the western flanks of Yucca Mountain, Nevada, the proposed site of the nation's first high-level radioactive nuclear waste repository. A set of the most fragile geological features found to date are detailed and digital representations are developed in this report. Their fragilities when shaken by representative ground motions are determined via three-dimensional rigid-block simulations using the custom built code *Rigid*. This code is described and some results are compared and validated with previous work. The fragilities are presented for use, in conjunction with feature residence estimates, to test and constrain ground motion estimates over long time periods.



## **ACKNOWLEDGMENTS**

This work was supported by the Pacific Earthquake Engineering Research Center's Lifelines Program funded by the Pacific Gas and Electric Company and California Department of Transportation. Any opinions, findings, and conclusions or recommendations expressed in this material are those of the authors and do not necessarily reflect those of the sponsoring agencies. Special thanks to Drs. Thomas Hanks and Norman Abrahamson for their continued support of this project.



# CONTENTS

ABSTRACT.....	iii
ACKNOWLEDGMENTS .....	v
TABLE OF CONTENTS .....	vii
LIST OF FIGURES .....	ix
LIST OF TABLES.....	xiii
<b>1 INTRODUCTION.....</b>	<b>1</b>
<b>1.1 Precarious Rock Constraints on Extreme Ground Motions.....</b>	<b>1</b>
1.1.1 Precarious Rocks at Yucca Mountain .....	2
<b>1.2 Previous Methods of Fragility Determination.....</b>	<b>4</b>
<b>2 METHOD FOR THREE-DIMENSIONAL FRAGILITY</b>	
<b>DETERMINATION OF GEOLOGICAL FEATURES.....</b>	<b>5</b>
<b>2.1 Field Studies .....</b>	<b>5</b>
2.1.1 Survey for Fragile Geologic Features .....	5
2.1.2 Age Dating .....	7
<b>2.2 Delineation of Fragile Geologic Features.....</b>	<b>7</b>
<b>2.3 The Discrete Element Method and the <i>Rigid</i> Implementation.....</b>	<b>11</b>
2.3.1 <i>Rigid</i> Overview .....	15
<b>2.4 Comparison with 3DEC .....</b>	<b>18</b>
<b>3 NUMERICAL ANALYSES .....</b>	<b>21</b>
<b>3.1 Objects Selected for Analyses .....</b>	<b>21</b>
<b>3.2 Comparison with Andrews et al. [2007] Ground Motions .....</b>	<b>32</b>
<b>3.3 Comparison with Wong Waveforms.....</b>	<b>33</b>
<b>3.4 Waveforms Selected for Fragility Analyses.....</b>	<b>36</b>
<b>3.5 Validation Exercise .....</b>	<b>42</b>
<b>3.6 Fragility Results .....</b>	<b>45</b>
REFERENCES.....	47
APPENDIX.....	49



## LIST OF FIGURES

Figure 1.1	Location map for precarious rocks. Most of the rocks are on the western slope of Yucca Mountain in Solitario Canyon.....	2
Figure 1.2	A view of Solitario Canyon and Yucca Mountain. Most of the fragile geological features are found along the middle ledge of the western face of Yucca Mountain (inset).....	3
Figure 2.1	Examples of different PBR classification. The free-standing rock in the upper left (Class 1) is not in place. This is evident from the orientation of the lithophysae in the rock. The other geologic features (Class 2-4) shown here have become fragile in place.....	6
Figure 2.2	Usage of targets and printed fabrics on rocks, as part of the photogrammetry process. The axis system mounted atop of a tripod is visible in the photograph on the right. ....	9
Figure 2.3	Examples of rock shapes determined by photogrammetry. ....	10
Figure 2.4	Rigid user interface. ....	15
Figure 2.5	The object model components. ....	17
Figure 2.6	A test model of a geode bouncing on a flat surface with gravity. ....	19
Figure 3.1	Location map for the PBRs studied in this project. The photographs, counter-clockwise, are class 2 features (free-standing <i>in-place</i> single rocks): Nichole (a), Matt Cubed (b), Sue (c), Pillow (d), S_Yucca_2 (e), and Fluffy (f), and class 3 features ( <i>in-place</i> rock stacks): Len (g), Whitney (h), and Tripod (i).....	22
Figure 3.2	Fluffy is a Class 3 feature that is located at a distance of about 0.58 km from the Solitario Canyon Fault. It is composed of two separate pieces that rest on a relatively flat ground surface. The combine height is about 1.1 m. Photographs taken from different angles are shown next to the corresponding orientations of the 3D shape used in the numerical simulations. ....	23
Figure 3.3	Len is a Class 3 stack of rocks that is located in the middle ledge of the Western slope of Yucca Mountain at a distance of about 0.81 km from the Solitario Canyon Fault. The stack is about 2.7 m high and is composed of several separate rocks that lean eastward, against the mountain side. Only the top 5 pieces have been modeled in this study. Photographs taken from different angles are shown next to the corresponding orientations of the 3D shape used in the numerical simulations.....	24

Figure 3.4	Matt Cubed is a Class 2 rock that is located in the middle ledge of the Western slope of Yucca Mountain at a distance of about 0.65 km from the Solitario Canyon Fault. It is a 1-m-high rectangular-shaped rock that sits against the mountain face. Photographs taken from different angles are shown next to the corresponding orientations of the 3D shape used in the numerical simulations. ....	25
Figure 3.5	Nichole is a Class 2 rock that is located in the middle ledge of the western slope of Yucca Mountain at a distance of about 0.74 km from the Solitario Canyon Fault. This the northernmost rock studied here. Photographs taken from different angles are shown next to the corresponding orientations of the 3D shape used in the numerical simulations. ....	26
Figure 3.6	Pillow is a Class 2 rock that is located near the foot of Yucca Mountain. It has a height of about 0.5 m and is at about 0.53 km from the Solitario Canyon Fault. Photographs taken from different angles are shown next to the corresponding orientations of the 3D shape used in the numerical simulations. ....	27
Figure 3.7	S-Yucca_2 is a Class 2 rock that is located in the middle ledge of the western slope of Yucca Mountain at a distance of about 0.54 km from the Solitario Canyon Fault. This the southernmost rock used in this study. This is a fairly fragile rock that could topple in almost every direction, except for a small rock at one corner that restricts its motion. Photographs taken from different angles are shown next to the corresponding orientations of the 3D shape used in the numerical simulations. ....	28
Figure 3.8	Sue is a Class 2 rock that is located in the middle ledge of the western slope of Yucca Mountain at a distance of about 0.64 km from the Solitario Canyon Fault. Although this is not very fragile, its location on a high pedestal suggests of a very long age. Photographs taken from different angles are shown next to the corresponding orientations of the 3D shape used in the numerical simulations. ....	29
Figure 3.9	Tripod is a Class 3 stack of rocks that is located in the middle ledge of the Western slope of Yucca Mountain at a distance of about 0.68 km from the Solitario Canyon Fault. This very fragile stack is about 1.8 m high and is composed of four rocks. It rests on a pedestal that is also unstable. Photographs taken from different angles are shown next to the corresponding orientations of the 3D shape used in the numerical simulations. ....	30
Figure 3.10	Whitney is a Class 3 stack of rocks that is located in the middle ledge of the Western slope of Yucca Mountain at a distance of about 0.65 km from the Solitario Canyon Fault. This very fragile stack is about 1.3 m high and is composed of three rocks. It rests on a sloping pedestal. A small rock, wedged between one of the rocks and the pedestal prevents the stack from collapse. Photographs taken from different angles are shown next to the corresponding orientations of the 3D shape used in the numerical simulations. The wedge is shown in blue color. ....	31

Figure 3.11	The rectangular block models for validation exercise imported into <i>Rigid</i> .....	42
Figure 3.12	Fragilities for the rectangular blocks shown in Figure 3.2 obtained from the waveforms used in shake-table experiments. ....	44
Figure 3.13	The difference of the median Purvance et al. [2008] derived overturning probabilities and those obtained via <i>Rigid</i> . ....	44
Figure 3.14	Overturning fragilities for class 2 rocks Fluffy, Matt Cubed, Nichole, Pillow, Sue, and S_Yucca2, and Class 3 rock stacks Len, Tripod, and Whitney. ....	46



## LIST OF TABLES

Table 3.1	List of the geological features studied. ....	21
Table 3.2	Overturing analyses of geological features listed in Table 3.1 subjected to both subshear and supershear scenarios of Andrews et al. [2007]. ....	32
Table 3.3	Overturing results for the $10^{-5}$ exceedance ground motions at Point B. ....	34
Table 3.4	Overturing results for the $10^{-5}$ exceedance ground motions at Point B multiplied by a factor of two. ....	34
Table 3.5	Results for the $10^{-6}$ annual exceedance probability waveforms for Point B. ....	35
Table 3.6	List of waveforms selected for fragility analyses. ....	37



# 1 Introduction

Probabilistic seismic hazard analysis (PSHA) is based on statistical assumptions that are very questionable when extended to very low-probability maximum ground motions. Based on the 1998 PSHA [Stepp et al. 2001] for Yucca Mountain, Nevada, the predicted maximum ground motions at low annual probabilities of  $10^{-6}$  to  $10^{-8}$  are of the order of 10g acceleration and 10 m/sec velocity. The short historical database for instrumental recordings is not sufficient to determine the uncertainties in the statistical assumptions. This suggests that we look for geomorphic and geologic evidence constraining ground motions over long periods in the past. Since the extrapolated ground motions are so large, we might expect to find evidence for them if they have occurred in recent geologic time. Evidence considered here includes precariously balanced rocks and fragile stacks of rocks found in Solitario Canyon, along the middle ledge of the west face of Yucca Mountain.

## 1.1 PRECARIOUS ROCK CONSTRAINTS ON EXTREME GROUND MOTIONS

Naturally evolved precariously balanced rocks (PBRs) in the vicinity of seismically active faults have been used to provide constraints on the level of ground motions that have occurred during the time the rocks have been in their current positions [Brune 1996]. The relatively large horizontal ground accelerations predicted by the PSHA at Yucca Mountain [Stepp et al. 2001] are not consistent with the preliminary results from the precarious rock survey conducted by Brune and Whitney [2000], or the results described in Anooshehpour et al. [2004]. The importance of the precarious rock approach is that it gives a direct indication of maximum levels of ground shaking that a given location has experienced over time periods of thousands to tens of thousands of years. This is in sharp contrast to the indirect inferences drawn from PSHA.

Purvance [2005] has shown that PBRs overturn systematically when exposed to horizontal shaking. Overturning is found to be a function of rock size, rock shape, and excitation intensity. Purvance [2005] found that precariously balanced rocks overturn as a result of both high peak ground acceleration (PGA) and higher low-frequency content—either peak ground velocity (PGV), spectral acceleration at 1 sec [ $S_a(1)$ ], or spectral acceleration at 2 sec [ $S_a(2)$ ]. The derived formulation compares favorably with the results of shake-table tests of simple blocks. Purvance et al. [2006] has refined this methodology via a simply realized physical experiment to better predict the overturning responses of complex stone boulders similar to actual PBRs. These results constitute an important enhancement in the ability to effectively quantify the overturning potential of PBRs. Purvance [2005] additionally demonstrated a methodology to compare the PBRs with ground motion models derived from PSHA calculations.

### 1.1.1 Precarious Rocks at Yucca Mountain

As a result of the discovery of numerous PRBs in the vicinity of Yucca Mountain, particularly in Solitario Canyon (Figure 1.1), a methodology was developed to use these rocks as constraints on the probable ground motion to be expected at the designated national high-level radioactive-waste repository [Brune and Whitney 2000; Anooshehpour et al. 2004; Anooshehpour et al. 2006].

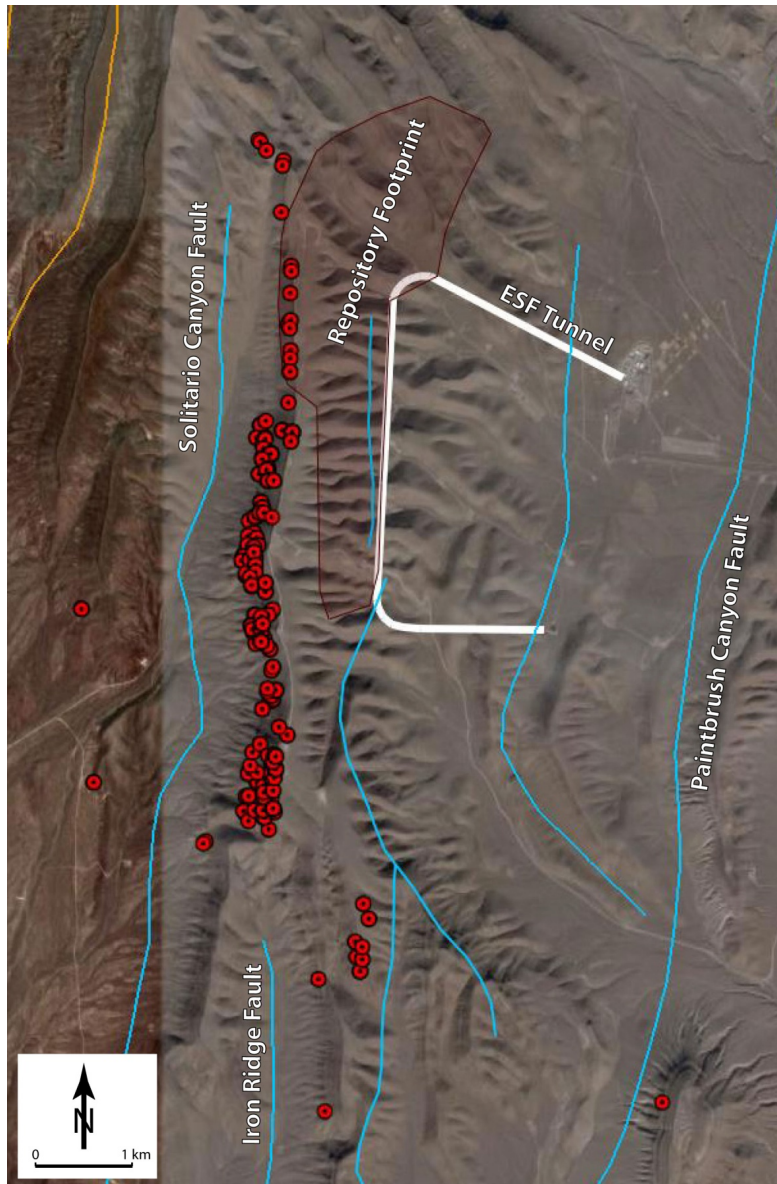


**Figure 1.1** Location map for precarious rocks. Most of the rocks are on the western slope of Yucca Mountain in Solitario Canyon.

The precarious rock methodology gives a direct indication of the upper bound on the amplitude of past ground shaking at a site; this is in contrast to the indirect inference provided by the extensive trenching studies at Yucca Mountain, which cannot directly constrain characteristics of ground motions associated with observed fault slip evidence. Brune and

Whitney [2000] concluded that the precarious rock data were consistent with the estimated age of the most recent large event on the Solitario Canyon fault (about 70 ka). The ground accelerations predicted by the Yucca Mountain PSHA [Stepp et al. 2001] were suggested by Brune to be inconsistent with the preliminary results from the precarious rock surveys, however. This conclusion was reiterated in the results described in the DOE Technical Report by Anoshehpour et al. [2002]. Therefore, it was concluded that further study of the precarious rock data had the potential of providing important constraints on the statistical assumptions, which lead to extremely high ground motion predictions at very low probabilities.

The objective of this work is to develop fragility models for selected precarious rocks at Yucca Mountain that can then be used to define the unexceeded ground motions at Yucca Mountain.

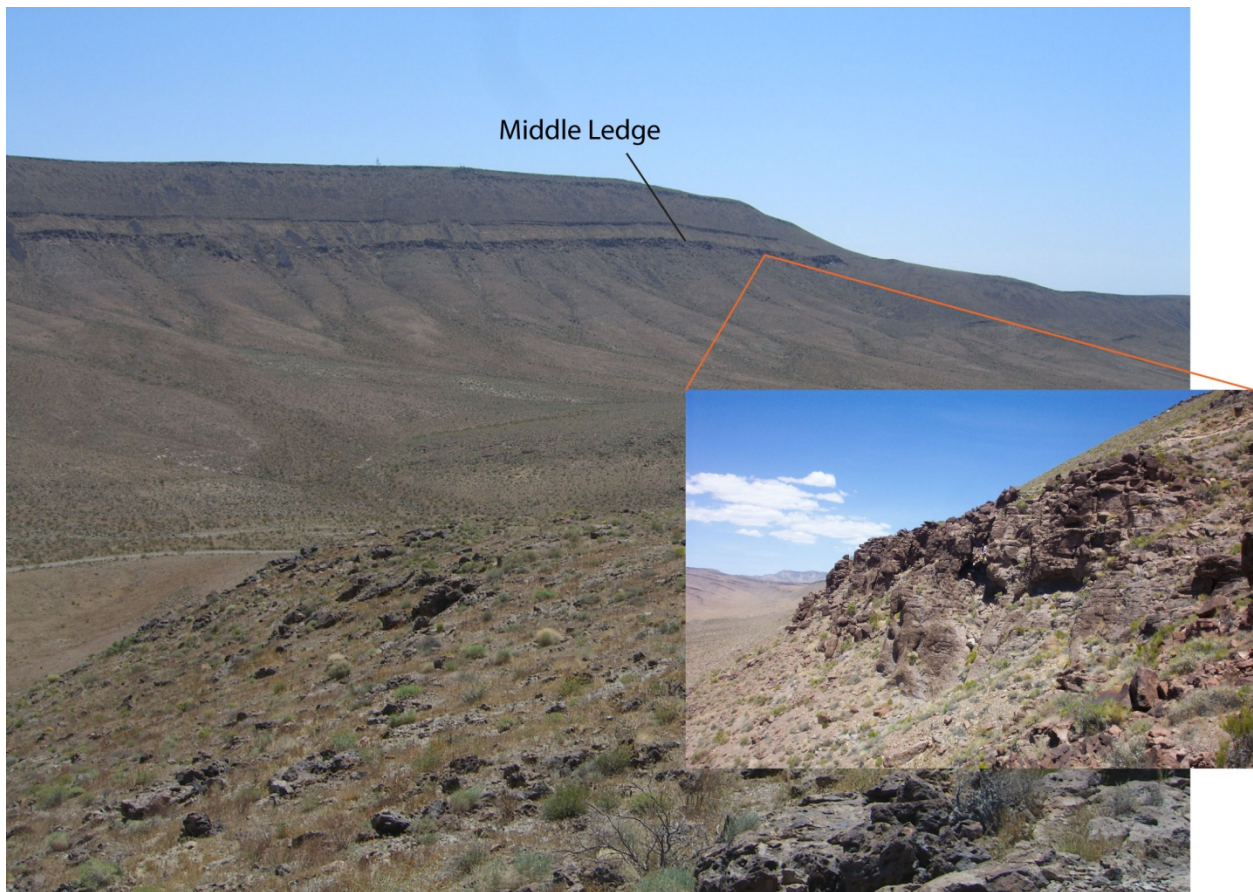


**Figure 1.2** A view of Solitario Canyon and Yucca Mountain. Most of the fragile geological features are found along the middle ledge of the western face of Yucca Mountain (inset).

## 1.2 PREVIOUS METHODS OF FRAGILITY DETERMINATION

Purvanche et al. [2008] documented the results of numerous computer simulations of the rocking and overturning responses of both symmetric and asymmetric two-dimensional blocks. This model assumed friction sufficient to inhibit sliding, the absence of free-flight or bouncing, horizontal forcing, and angular momentum preservation. Angular momentum preservation enforces a coefficient of restitution that depends on the block geometry. This is necessary as without bouncing, an unrealistic amount of energy persists in that two-dimensional (2D) model. Purvanche et al. [2008] validated the resulting parameterization of the overturning fragilities via shake-table tests of rocks similar to PBRs shaken in a unidirectional fashion. Initial estimates of the overturning fragilities of PBRs at Yucca Mountain, used in Anooshehpour et al. [2006], were based on the Purvanche et al. [2008] methodology. Anooshehpour et al. [2006] used forced tilting tests and field estimation to delineate the PBR geometrical parameters and contact conditions. Those PBR fragility estimates were added to the “Points in Hazard Space” [Hanks and Abrahamson 2010] graph as constraints on the Yucca Mountain seismic hazard curves of Stepp et al. [2001]. The preliminary analyses of Purvanche and Brune [2007] suggest that the PBRs are inconsistent with the Yucca Mountain PSHA.

Many of the PBRs at Yucca Mountain have quite complex geometries and are composed of numerous components (e.g., multiple stacked blocks). In some cases, failure may not result from rocking motion but may be more likely due to sliding. The Purvanche et al. [2008] methodology cannot account for such cases. Purvanche and Brune [2007] preliminarily used the 2D Itasca Consulting Group code UDEC [2009] to investigate 2D models with more complex geometries for Yucca Mountain PBRs. Those analyses included preliminary investigations of the effects of joint orientations on jointed cliff fragilities as those features are ubiquitous along Yucca Mountain. Purvanche and Brune [2007] found that the Yucca Mountain ground motions of Stepp et al. [2001] that occur every 100,000 years or greater would destroy 2D cliff models with realistic joint orientations. Those modeling efforts contributed substantially to our understanding of complex object fragilities and suggested that future work must account for both three-dimensional (3D) geometries and ground motions. To date, no 3D PBR fragility estimates have been obtained nor presented.

The Itasca Consulting Group code 3DEC [2008] was also investigated as a source for calculating 3D fragility estimates. That work was guided to some degree by the effort of Psycharis et al. [2003] and others who used 3DEC to simulate the rocking and overturning responses of classical columns. Upon further investigation, 3DEC was deemed unsuitable for these analyses. This conclusion was based on the following reasons: (1) computational efficiency; (2) idealization of the moment of inertia tensor; (3) lack of a simple/efficient method to implement contact restitution; and (4) accuracy. The presentation below will discuss using the discrete element method and present the justifications for these conclusions. In addition, the form of the rigid block modeler *Rigid* will be outlined.

## **2 Method for Three-Dimensional Fragility Determination of Geological Features**

Estimates of fragility of geological features in seismically active regions provide physics-based constraints on maximum ground motions at low probabilities. As part of this work, a 3D computer code was developed that uses the data obtained in field studies to calculate fragilities of geological features. A description of this method is presented in the following sections.

### **2.1 FIELD STUDIES**

Field studies included surveying for fragile geologic features, collecting samples from rock surfaces to estimate the age of the rocks and erosion rates, taking multiple pictures of the objects for shape determination using photogrammetry, and, when necessary, conducting forced tilting tests of the freestanding rocks to obtain quasi-static toppling accelerations.

#### **2.1.1 Survey for Fragile Geologic Features**

Near Yucca Mountain there are many spectacular precariously balanced boulders that are covered with dark rock varnish. The darkness of the rock varnish (a subaerially deposited coating of manganese and iron oxides, clay minerals, and organic matter) on many of these boulders suggests that they have been in these positions for more than 10 ka and perhaps several tens of thousands of years. Figure 1.1 shows the locations of the surveyed precarious rocks near Yucca Mountain. Nearly all are located on the western slope of the main ridge at Yucca Mountain, the footwall of the Solitario Canyon Fault.

Several precarious rocks were found on Jet Ridge, west of Yucca Mountain. Such rocks appear to be fewer in number at this locality than in Solitario Canyon. Farther west, on West Ridge and in northern Crater Flat, precarious rocks were not found during a reconnaissance inspection. A small number were observed in Fortymile Wash and in Yucca Wash, but weathering and erosion of most of the volcanic outcrops on the north side of Yucca Wash does not appear to produce precarious rocks.

The old basalt flows and cones in southern Crater Flat between Solitario Canyon and Lathrop Wells have a number of semi-precarious rocks. Bare Mountain is composed primarily of formations (Paleozoic and Precambrian sedimentary and metasedimentary rocks) that do not appear to form precarious rocks, with the exception of a few that formed in basalt dikes at the mouth of Tarantula Canyon. There are a number of precarious rocks in Fluorspar Canyon at the north end of Bare Mountain, in non-welded tuff just north of Crater Flat, in Busted Butte, and in Beatty Wash and Fortymile Wash.

### 2.1.1.1 Classification of Fragile Geological Features at Yucca Mountain

We have classified fragile geological features at Yucca Mountain into four groups (Figure 2.1):

- Class 1: Free-standing rocks that are not in place. These may be the most fragile features on Yucca Mountain, but the age of these rocks are the most difficult to determine or defend.
- Class 2: Free-standing rocks that are in place.
- Class 3: Free-standing or leaning stacks of rock that are in place.
- Class 4: Cliffs.

Nearly all the precarious rocks in this study have been eroded from jointed, densely welded tuff, which weathers very slowly in the dry semi-desert of the southern Great Basin. Welded tuff does not weather into small fragments but typically breaks up into large boulders that maintain rectilinear shapes inherited from original jointing.

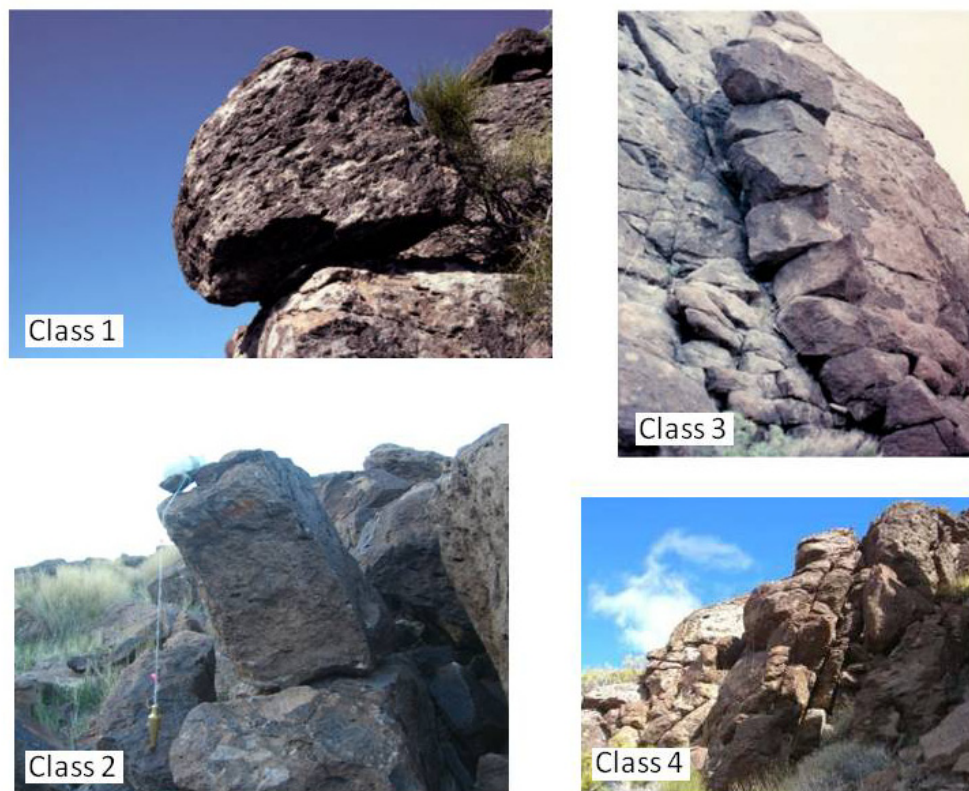


**Figure 2.1** Examples of different PBR classification. The free-standing rock in the upper left (Class 1) is not in place. This is evident from the orientation of the lithophysae in the rock. The other geologic features (Class 2-4) shown here have become fragile in place.

Boulders may become precariously balanced by root activity, freezing and thawing, and possibly other geomorphic and weathering processes. Wedging by root activity and freezing leads to opening of cracks and filling with fine material moving downslope from above. Erosion may then proceed to the point that blocks of rock become nearly unconfined; the fine material is washed out, leaving the rocks in isolated precarious positions [Brune 1996].

### 2.1.2 Age Dating

Many of the balanced rocks in this study area are partially or completely coated with rock varnish. Some of the darkest rock varnish analyzed from surface boulders on Yucca Mountain hillslopes indicates that surface-exposure ages can exceed 100 ka [Stepp et al., 2001]. The darkness of the rock varnish on many of the boulders in this study suggests that they have been in these positions for more than 10 ka and probably several tens of thousands of years. This is confirmed by the age dates obtained by Bell et al. [1998] for rock varnish layering and by more recent cosmogenic age dates and estimates of landscape evolution in the vicinity of Yucca Mountain [Rood 2009]. The high slope stability, as evidenced by the preservation of middle Pleistocene deposits on Yucca Mountain hillslopes, is consistent with the relatively long-term stability of precarious rocks.

## 2.2 DELINEATION OF FRAGILE GEOLOGIC FEATURES

In order to ascertain the ground motion amplitudes required to overturn a 3D object, one must accurately assess both the object geometry and the geometries/characteristics of any possible contacts. Object geometry delineation has been achieved via the commercial software package *PhotoModeler* (<http://www.photomodeler.com/index.htm>) (see Appendix). *PhotoModeler* is a photogrammetry implementation wherein multiple pictures of a scene are taken from different vantage points, common points are selected between the different views, and camera positions/orientations are estimated. The *PhotoModeler* package provides a simple method to calibrate any digital camera in order to ascertain characteristics such as focal length and edge distortion. The calibration process involves capturing pictures of a projected grid of points from different orientations and solving for the pertinent camera parameters.

An inexpensive Casio EXILIM handheld digital camera has been calibrated and used for all Yucca Mountain-related analyses. Common points between multiple pictures were selected and referenced within the *PhotoModeler* application. The co-referenced points were used along with initial camera location estimates as inputs to an iterative solver; this solver minimizes an estimate of the global point location error. This process results in relatively high-quality 3D camera locations that are the basis of the 3D object representations. In general, this process will lead to 3D models in which modeled object points are located to within ~1% of their true locations (for discussions of model accuracy see technical reports in [http://www.photomodeler.com/applications/articles\\_and\\_reports.htm](http://www.photomodeler.com/applications/articles_and_reports.htm)). An axis system mounted atop a tripod has been created to provide both length scales to the *PhotoModeler* projects along with 3D orientations (Figure 2.2). Orientation relative to vertical is essential in these analyses as the center of mass of an object must not exceed the vertical projection of the contact points in order for the object to remain stable. This method allows one to determine object points (3D points obtained after processing a *PhotoModeler* project) and a representative object model (an abstraction of these points into a closed 3D polyhedron).

The object point locations are sparse representations of the object geometry. Ubiquitous, dense (less than a few decimeters) object point coverage has not been sought as the constituent pieces of the objects are approximated as convex polyhedra. *PhotoModeler* provides an automatic triangulation tool that produces a triangularly faceted, convex hull based on selected object points. In general, a 3D convex hull is the most tightly fitting convex 3D surface that surrounds a set of points. As a result, the triangularly faceted convex hull of a constituent piece,

heretofore referred to as an object component model, is an idealization of some portion of a physical object.

For instance, a fragile stack of boulders may consist of a number of individual rocks in contact with one another. In this case an object component model is created for each rock in the stack. Should an individual object component have a large degree of concavity, it is possible to split the object points into subsets that are convex generating multiple convex object models for that component. These models can be combined into one object component model, reproducing a closer approximation to the concave geometry. This has not been necessary as the object components investigated in this work are convex or nearly convex. The resulting 3D object component models are output as ASCII stereolithography (.stl) files. Thus for a stack of rocks a '.stl' file exists for each rock (object component) of the stack. At a minimum, a total model fit for fragility computation includes component models of both the object and the pedestal upon which it rests. Anooshehpour et al. [2007] used the *PhotoModeler* method outlined above to obtain volume estimates of test rocks with known weights similar to rocks found on Yucca Mountain. That study found that the *PhotoModeler*-based method using the same Casio EXILIM camera was able to reproduce rocks volumes to within a few percent of the actual volumes. Thus there is a high degree of confidence that the object geometries have been gauged in an accurate fashion.

Accurate assessments of the contact conditions/geometries between contacting objects are also required for accurate fragility analyses. These are very difficult to ascertain without moving the objects in question and inspecting the contact geometries in great detail. In many cases at Yucca Mountain such an invasive investigation would lead to permanent object failure. Also such in-depth scrutiny of contact conditions on the flanks of Yucca Mountain is not feasible without significant effort. As a result, the *PhotoModeler*-based object component models have been slightly augmented when necessary to produce contact configurations that are consistent with the available data. These fine adjustments have been accomplished using the Google SketchUp (<http://sketchup.google.com/>) software package. This freely available package allows one the ability to create and modify 3D representations of objects. Two additional plugins have been utilized to import/export .stl files into and out of Google SketchUp (import: <http://www.crai.archi.fr/RubylibraryDepot/Ruby/su2stl.rb> and export: <http://www.guitar-list.com/download-software/convert-sketchup-skp-files-dxf-or-stl?page=9>).

Once the *PhotoModeler*-based files have been imported, they can be closely inspected and modified. Object component models have been modified as follows: (1) add vertices to existing triangularly faceted surface representations for more accurate contact modeling in *Rigid*; and (2) augment contact configurations to produce more realistic geometries. Point (1) will be discussed in more detail in the discussion of *Rigid*. Point (2) is required as the real contact configurations are not always convex. In these cases, the boundary representation obtained from *PhotoModeler* may not be realistic due to the convex hull calculation. These unrealistic contact configurations can result in the inability to equilibrate the *Rigid* model prior to fragility calculations or unrealistically precarious fragilities. As a result, the model boundaries have been slightly modified to create more realistic and more stable contact configurations.

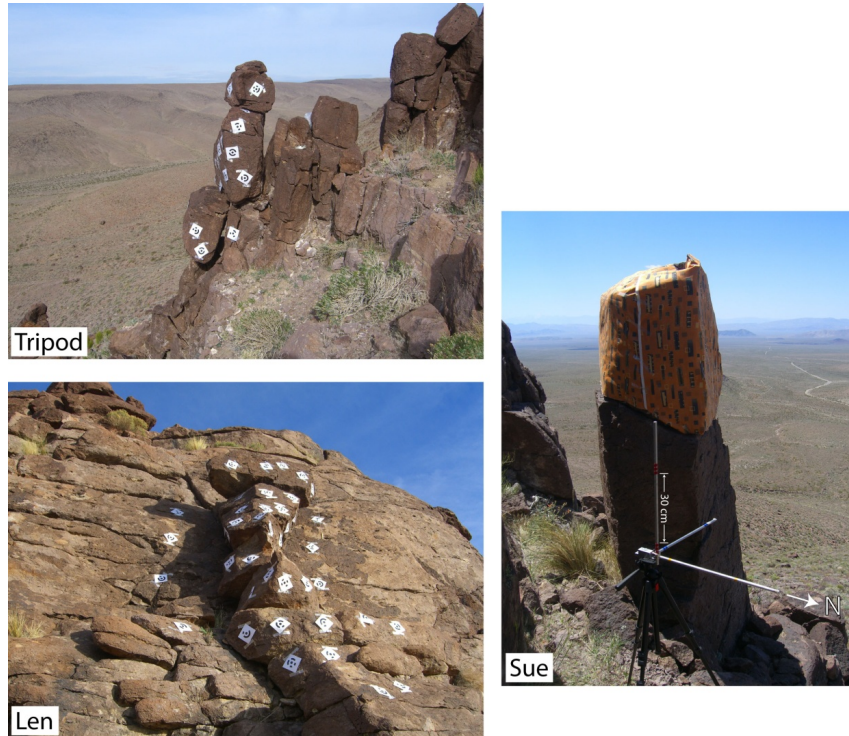


**Figure 2.2** Usage of targets and printed fabrics on rocks, as part of the photogrammetry process. The axis system mounted atop of a tripod is visible in the photograph on the right.

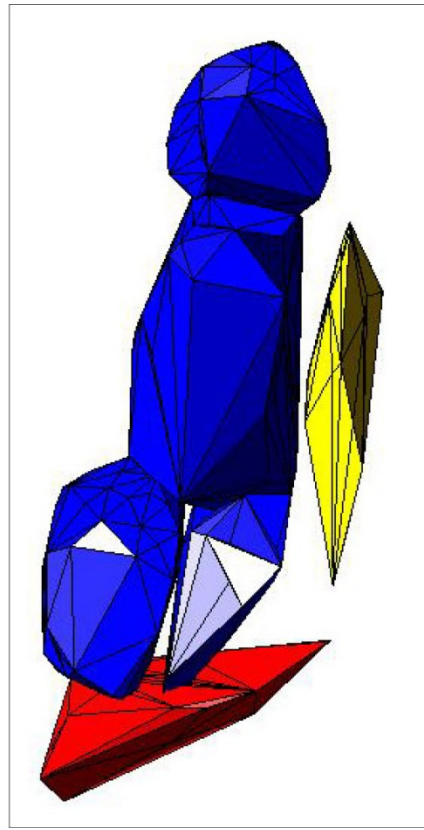
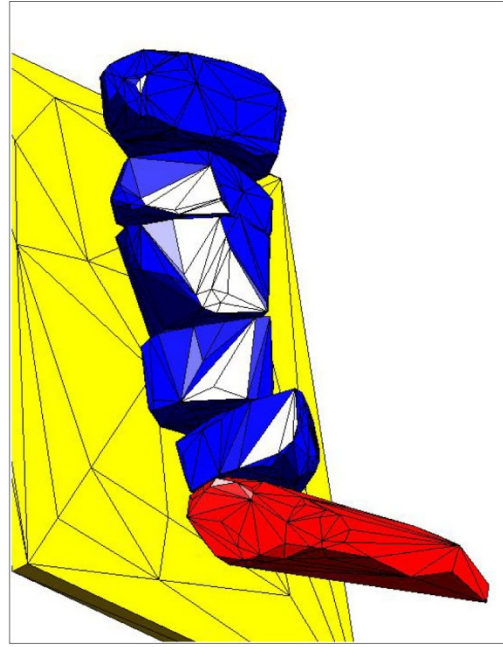


**Figure 2.3** Examples of rock shapes determined by photogrammetry.

## 2.3 THE DISCRETE ELEMENT METHOD AND THE RIGID IMPLEMENTATION

The Discrete Element Method (DEM), first introduced by Cundall [1971], simulates the response of large rock units consisting of numerous component blocks. The DEM has flourished since that pioneering work, and numerous efforts have been devoted to many aspects of the DEM. In fact, the Web of Science database holds more than 1200 peer-reviewed journal article references involving DEM technologies ([http:// www.isiknowledge.com/](http://www.isiknowledge.com/) last visited on 11/30/2009, search “discrete element method”). Cundall and Strack [1979] and Cundall [1988] further delineated the details of DEM and outlined the specifics of a DEM model for particles or blocks. In general, a DEM model consists of either rigid or deformable entities with discrete boundaries that interact with one another through contacts. Contacts are formed when these entities touch one another; slight overlap of contacting entities is allowed in DEM simulations. This soft contact approach essentially places a spring (and perhaps dashpot) at the contacting points. These notional springs form the basis for force/moment transmission between objects. Thus the DEM scheme must efficiently detect contacts between any objects that exist in the model space and efficiently resolve the appropriate contact forces. These two tasks—contact detection and resolution—are major computational tasks and require robust algorithms. Once the forces and moments of all objects in the model domain have been updated, the equations of motion must be solved, updating the object locations. The calculation step requires contact detection, force/moment updating, and location updating.

One of the primary breakthroughs outlined in Cundall [1988] is the concept of a common plane ( $c-p$ ). In general, detecting contacts between 3D polyhedral blocks via brute force methods consumes a significant amount of computational time, especially for complex polyhedra. The  $c-p$  approach considerably increases contact detection efficiency and creates a robust framework for assigning the direction normal to a contact. Cundall [1988] defines a  $c-p$  as “a plane that, in some sense, bisects the space between the two contacting particles.” One can imagine that the  $c-p$  is a sheet of metal that exists between two convex blocks. Bringing the blocks together, the metal sheet would be deflected and trapped, defining the direction that the blocks would slide relative to one another. This is the exact information required to robustly define the contact normal between convex blocks. In DEM, blocks slightly overlap one another when in contact, and the  $c-p$  is placed so that one minimizes the gap between the common plane and the vertex that is most deeply overlapping the other block. Thus, given a valid  $c-p$ , it is easy to detect contacts since contacting objects must both intersect the  $c-p$ . In addition, a robust contact normal can be defined between contacting convex objects that is the normal to the  $c-p$ . This  $c-p$  concept has been amazingly versatile, leading to many advances in computational mechanics. The efficiency of  $c-p$  determination is paramount in DEM simulations as contact detection and resolution can constitute up to 70–80% of the total analysis time [Nezami et al. 2006].

The Cundall [1988] method for determining the  $c-p$  is the approach utilized in 3DEC [Itasca Consulting Group 2008]. Initial  $c-p$  estimates are created based on the block geometries. Subsequently the  $c-p$  is translated to produce the maximum gap between the  $c-p$  and the closest vertices of each block for non-contacting blocks. For blocks in contact, the translation minimizes the overlap between the deepest vertex and the  $c-p$ . Once translated, a reference point is chosen on the  $c-p$  and the plane is iteratively rotated about this point in order to find the maximum gap (or minimum overlap). The rotations of the  $c-p$  about the reference point are accomplished iteratively as the closest vertices of a block to the  $c-p$  that can change as the  $c-p$  is rotated. A number (perhaps large) of rotations are required to ensure that the gap estimate is a maximum (overlap estimate is minimum), and the closest vertices to the  $c-p$  are continuously updated. This

iteration stops when small perturbations to the  $c-p$  orientation produce smaller gaps or larger overlap values. Should a vertex lie within a predefined tolerance of the  $c-p$  or on the side opposite of the center of mass of the block to which it belongs, the blocks are deemed in contact and the appropriate reaction forces can be calculated and applied.

Nezami et al. [2004] demonstrated a method to determine the  $c-p$ , termed the fast common plane (FCP) approach, which they found to be up to 40 times faster than the Cundall [1988] method. Later Nezami et al. [2006] introduced the shortest link method (SLP), an improvement on the FCP method. They demonstrated a consistent speedup factor of 18 relative to the Cundall [1988] iterative approach for a system composed of numerous polyhedral blocks. As a result, the SLP method has been implemented in *Rigid*. Nezami et al. [2006] demonstrated that the  $c-p$  between non-contacting, convex, polyhedral blocks is defined by the line connecting the closest points on the surfaces of the blocks (the shortest link). The contact normal in this case is defined as the direction of the shortest link. The shortest link computation for non-contacting blocks can be efficiently implemented should the blocks be discretized into triangular facets. The data structures used in *Rigid* are designed exclusively for triangularly faceted polyhedral, where there exist facets, vertices (3 per facet), and edges (3 per facet). The equations of a 3D triangle can be formed and solved very efficiently in order to find the closest point on a triangle to an arbitrary point in space. Should one have the ability to find the closest point on a convex block to a point in space, it is not hard to imagine an iterative scheme for finding the closest points on block surfaces. Suppose one starts with an initial point on the surface of block1. Once the closest point on block2 to the initial point on block 1 has been determined, one can reset the initial point as the closest point on block2 and search for the closest point on block1. This iterative process is halted when the absolute locations of the closest points do not change to within a specified tolerance. There are a few degenerate cases that must be taken into account as outlined by Nezami et al. [2006], but these cases are easily handled.

Finding the closest point on a convex block to a given 3D point requires a mechanism to traverse the data structures in a coherent and efficient fashion. A brute force method would be to find the closest points on each of the block facets to the given point, selecting the one with minimum distance. Instead, Nezami et al. [2006] suggested a scheme based on nearest neighbors. Suppose that an initial point is selected on block1 and a facet is selected on block2. This traversal relies on the determination of whether or not the closest point lies in the center of a facet, on a facet edge, or on a facet vertex. Should the closest point on block2 to the point on block1 lie on an edge but not a vertex, the neighboring facet on block2 to that edge is checked to see if the closest point on that facet is closer to the point on block1 than the previous closest point estimate. Should the closest point on block2 lie on a vertex, on the other hand, all neighboring facets to the vertex on block2 must be checked and the closest points calculated. When a new closest point on block2 is determined, tests for possible new closest points on block2 are undertaken. The traversal scheme terminates when the closest point on block2 does not lie on a vertex or an edge or when all of the neighboring closest point tests reveal distances from the initial point that are further than the current estimate. Once the closest point between block2 and the point on block1 has been determined, the process is repeated wherein the traversal occurs along the facets of block1 and the 3D point is the previous closest point estimate on block2, as discussed above.

The SLP method assumes that the blocks are not in contact or overlapping. Should the blocks overlap, an additional step is required to enforce separation. This is accomplished by translating the blocks in the direction of the previous  $c-p$  normal by a distance just sufficient to

ensure that they no longer overlap. The shortest link and  $c-p$  are determined for this displaced configuration. This method presumes that the model geometries vary a small amount during each time step of a calculation cycle, which is true for the DEM simulations undertaken here. The SLP method, as implemented in *Rigid*, has been tested for robustness via numerous block models interacting with one another.

The Cundall [1988]  $c-p$  approach has not been implemented in *Rigid*; therefore, it is difficult to compare the efficiency of the two schemes directly as other aspects of the computations are very different. For instance, Cundall [1988] introduces a method for detecting neighbor proximity for blocks so that a  $c-p$  is only determined between block pairs that are sufficiently close to one another. This is accomplished by partitioning the model domain into cubes and mapping the blocks into the cubes based on their Cartesian extents. Thus neighbors for which contact detection must occur must be mapped into the same cubes. When there are more than perhaps 100 blocks, the Cundall [1988] cell space method for neighbor identification outperforms an all-in-all comparison where a  $c-p$  is determined for each block-block pair. Such a cell space implementation has not been included in *Rigid* as its primary purpose is to simulate small assemblages of blocks such as those representing PBRs. In this case, an all-in-all comparison outperforms the cell space implementation. Thus although *Rigid* in its current form is not designed for large scale simulations of polyhedral granular assemblies, it is most efficient for the types of models representing fragile geological features on Yucca Mountain.

The  $c-p$ , as determined by the SLP method, provides a contact normal direction. Where are the contacts actually located, though? The contact locations are important as they constitute the locations where forces and moments are transmitted from one block to another and applied. *Rigid*, in a similar fashion to 3DEC, uses the concept of a subcontact to identify points of force transmission. Once objects are found to be in contact via the SLP method, all vertices of block1 that inclusively lie inside block2 and vice-versa are determined. Each vertex that passes this “is-inside” test is identified as a subcontact. All forces and moments are calculated and stored at the subcontact locations. Should no vertices of either block lie inside the other block, a subcontact is placed at the location of the closest point as determined by the SLP method. This degenerate case is important for edge-edge contacts and is handled naturally in *Rigid*. Subcontacts are deleted when the vertex that was previously inside the other block fails the is-inside test. An efficient method that calculates the signed volume of a triangular pyramid is used as the basis for the is-inside determination.

As in 3DEC, the relative velocity of the two blocks is determined at the subcontact location. *Rigid* assumes that the relative velocity is constant during a time step so that relative displacement can be determined. Both normal and tangential spring constants are used to calculate the incremental shear and normal forces (as defined by the  $c-p$ ) that are cumulatively summed. In this way one can easily enforce slipping conditions by limiting the shear force stored at a subcontact based on the coefficient of friction and the normal force. As noted in Guzzetti et al. [2002], when rocks collide with much force, significant damage may occur and the rebound velocity may be significantly diminished from the impact velocity. In order to account for this effect, *Rigid* uses the hysteretic damping model outlined in Lankarani and Nikravesh [1990]. Instead of a linear force-displacement response, the hysteretic model presumes that the normal force is proportional to the indentation (accumulated normal displacement) to the 1.5 power. Energy is dissipated during contact proportionally to the ratio of the impact velocity to the current relative contact velocity in a similar fashion to the Kelvin-Voigt damping model. Although the restitution coefficient (ratio of rebound to impact velocities) is not uniquely defined

by this model (except under very strong assumptions), the effect of this model is to dissipate energy during impacts in a physically sound fashion. This model is used extensively in contact mechanics simulations in engineering (see Gilardi and Sharf [2002] and references contained therein).

Once the subcontact lists and forces/moments have been updated, the subcontact forces/moments are summed for each block. Next, the equations of motion are solved and the block vertex locations are updated. The summed forces are presumed to act at the centroids of the blocks. The equations of motion involving linear momentum are discretized in a fourth order fashion and integrated via the Velocity Verlet method ([http://en.wikipedia.org/wiki/Verlet\\_integration](http://en.wikipedia.org/wiki/Verlet_integration)). This results in an update to the block centroid locations and linear velocities. The Velocity-Verlet method does not require knowledge of the state of the block (e.g., velocity or acceleration) from previous time steps to update the current values and is a common integrator in DEM simulations. The updates of location and velocity from time step  $t$  to  $t+dt$  occurs in four steps: (1) the position at time  $t+dt$  is calculated based on the current location, velocity, and acceleration; (2) the half-step velocity is calculated (at  $dt/2$ ) based on the current velocity and acceleration; (3) the acceleration at  $t+dt$  is updated from contact forces; and (4) the velocity at  $t+dt$  is updated via the newly calculated acceleration. This integrator presumes that the velocity is constant during  $dt$ . The Velocity-Verlet method is simple to implement, stable, and accurate. This integrator is very similar to the one implemented in 3DEC.

The 3DEC solves the equations of motion representing angular momentum in a very simplistic manner. Generally the three degrees of freedom for rotation are coupled so that a number of matrix multiplications are required for rotational motion updating. In order to avoid this overhead, 3DEC uses a reduced representation of the inertia tensor. Essentially the inertia tensor is diagonalized, and all of the coupling terms in the rotational equations of motion are discarded in 3DEC. Thus rotational motions that are not modeled correctly may impact the results of simulations where large rotations occur. In addition, 3DEC implements a second order integrator to update the rotational equations of motion.

As shown in Buss [2000], second order integrators of the form used in 3DEC are very poor performers when conservation of angular momentum is scrutinized. Although Buss [2000] investigated solving the full, coupled, rotational equations of motion, it is not clear whether or not these results apply to the reduced representation used in 3DEC. In order to provide a more robust and physically accurate representation, *Rigid* utilizes the full inertia tensors and a fourth order Runge-Kutta integrator to update the rotational equations of motion. The inertia tensor is determined based on the method outlined in Blow and Binstock (2004), which is simple to implement and very efficient. In order to avoid Gimbal lock (loss of a degree, of freedom during rotation, see [http://en.wikipedia.org/wiki/Gimbal\\_lock](http://en.wikipedia.org/wiki/Gimbal_lock)) and drift that can accrue when updating rotation matrices, the equations of motion have been cast in terms of quaternions.

Unlike Munjiza et al. [2003] and Johnson et al. [2008], the full quaternion representation is integrated in *Rigid* as the additional computational effort is relatively small. Rotations of block vertices are accomplished by converting the quaternion representation of the block configuration to a rotation matrix. This is more efficient than applying the quaternion rotations directly to the block vertices. As a result, copies of the block vertex lists are maintained relative to their original orientations about the block centroids. This practice also remediates vertex drift due to the accumulation of round off error.

### 2.3.1 Rigid Overview

*Rigid* has been constructed using Qt, a cross-platform user interface framework (<http://qt.nokia.com/products>). Qt is a free set of C++ libraries that facilitate the creation of applications. Currently *Rigid* is available as either 32- or 64-bit Windows applications. Figure 2.4 shows the *Rigid* user interface in its current form.

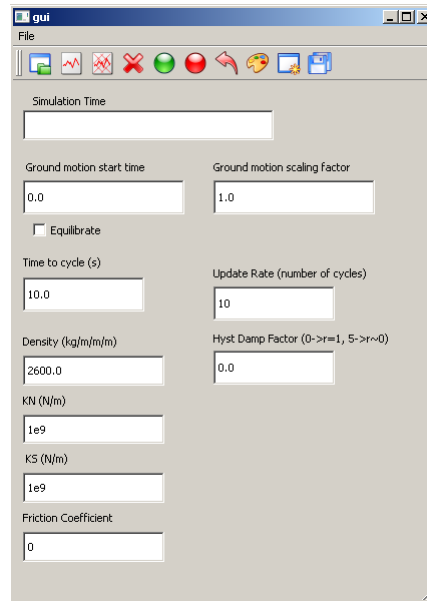


Figure 2.4 Rigid user interface.

Formatted text files are used to load a set of object component models into the simulation domain via the  button. An example of a formatted text file follows:

```
block fluffy_bot_rock.stl
0 0 0 0
block fluffy_top_rock.stl
0 0 0 0
block fluffy_pedestal.stl
1 0 0 0
```

The block identifier is used to tell *Rigid* that an .stl filename is going to follow. The following line holds an integer followed by three doubles. The integer (0 or 1) specifies whether a block is free to move (0) or fixed (1). If a waveform is loaded into *Rigid* for fragility estimation, the velocities of that waveform are applied to all fixed blocks in the model. Otherwise, fixed blocks do not move. Thus one can equilibrate a model to static equilibrium by cycling without loading a waveform. The following three doubles are the initial  $x$ ,  $y$ , and  $z$  velocities of the blocks as

defined in the .stl file. An initial velocity assigned to a fixed block is kept constant throughout the simulations. Note the formatted text file must be in the same directory as the .stl files.

The user interface provides one with the ability to change the physical parameters of the model. Note that the current *Rigid* implementation applies the same physical parameters to each block. These parameters include: density, normal stiffness ( $K_N$ ), shear stiffness ( $K_S$ ), coefficient of friction, and hysteretic damping coefficient. Throughout the simulations presented in this effort, the density is set to  $2600 \text{ kg/m}^3$ ,  $K_N = K_S = 10^{-8} \text{ N/m}$ ; the friction coefficient is set to 0.6, and the hysteretic damping factor is set to 2. This value of the hysteretic damping factor corresponds to a normal coefficient of restitution of roughly 0.2, but, as mentioned previously, it depends somewhat on the impact velocity. This relatively high degree of impact damping is consistent with the largest degree of damping seen in rock impacts, as outlined in Guzzetti et al. [2002].

Once an object model is loaded from the formatted text file, a plot window is automatically generated that renders each of the blocks. An example is shown in Figure 2.5 for the Len stack. The update rate dialog controls the rate at which the plot window is updated. Thus one can visualize the responses of the blocks as they are calculated. Note that it is much more efficient to close the plot window when cycling the model. The scroll bars at the bottom and right sides allow one to translate and zoom the plot item (bottom) along with rotate the plot item (right). Rotations are also possible by holding the left mouse button over the plot window and dragging the mouse. This interactive plot window is implemented in OpenGL and has been invaluable for model visualization and debugging. The axes are aligned with the  $x$ ,  $y$ , and  $z$  directions and the red crosses correspond to one-meter intervals. The  button returns the object model to its loaded state. It is also possible to save the current model state using the  button. This will generate a .msf file that holds all of the pertinent information to reload a model, including contact information and physical properties. This file must be located in the same directory as the .stl files for a model to be reloaded to a saved state. Thus the  button will also allow one to load .msf files. The program is terminated, including any open plot windows, with the  button, a new plot window is spawned with the  button, and the object model components are unloaded with the  button.

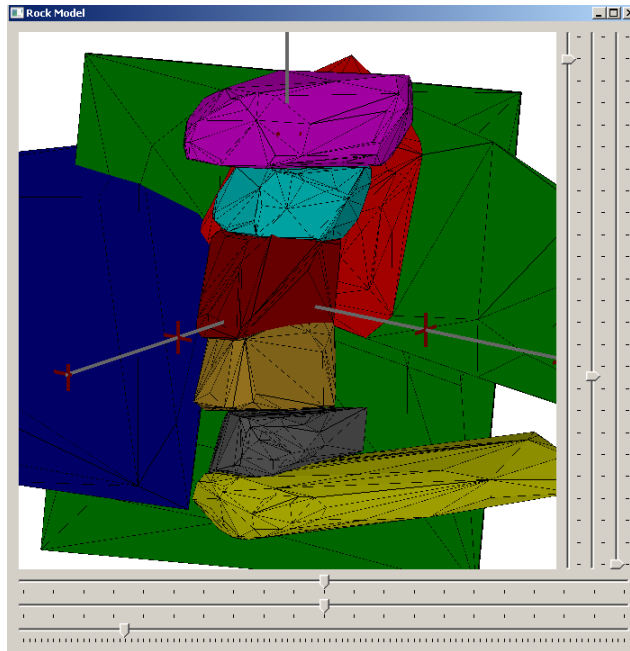


**Figure 2.5 The object model components.**

Ground motion time histories (acceleration records) are loaded via the  button. At this point only waveforms in the PEER strong-motion data format (.AT2 files) are allowed (see <http://peer.berkeley.edu/smcat/data.html> for this format and a library of strong ground motions in this format). Note that *Rigid* expects the filenames to be of the form XXX-X.AT2, XXX-Y.AT2, and XXX-Z.AT2 for the *x*, *y*, and *z* components, respectively. In addition, *Rigid* presumes that the *y* and *z* ground motion recordings have the same number of observation points as the *x* component and one must ensure that this is the case. The ground motion start time and ground motion scaling factor dialogs are useful when an .AT2 file has been loaded. Should one prefer to start the simulation at some time other than the beginning of the recording, they can enter a time in seconds in the ground motion start time dialog. Each ground motion component will be multiplied by the ground motion scaling factor. Note that the three component recordings must be in the same directory. A three-component ground motion recording is unloaded with the  button. The time to cycle dialog allows one to enter the number of seconds to simulate.

In addition, a batch file utility has been implemented so that the object models can be exposed to numerous ground motions in a batch fashion. The formatted text files (extension .ABF) are as follows:

```
0.05 0.1
0
059v2-X.AT2 13.7903 40.3341 0.06955 34.2635 0.50236
0637-X.AT2 2.477 12.0392 0.78317 72.6563 0.094602
```

Line 1 consists of scaling factors for PGA (in units  $g$ ) separated by spaces. Line 2 is deprecated and a 0 should be entered. Following these two lines is a list corresponding to each waveform. These lines include: the waveform filename (either the  $x$ ,  $y$ , or  $z$  name), beginning time (in seconds) for the simulation, ending time (in seconds) of the simulation,  $\text{GMRotI}_{\text{PGA}}$  ( $g$ ),  $\text{GMRotI}_{\text{PGV}}$  (cm/sec), and  $\text{GMRotI}_{\text{PGV}}/\text{GMRotI}_{\text{PGA}}$  (sec).  $\text{GMRotI}$ , as defined in Boore et al. [2006], is the median of the distribution of geometric mean peak amplitudes of a set of rotated horizontal components. In other words, one calculates the geometric mean of PGA of the two orthogonal horizontal ground motion recordings as they are rotated through  $90^\circ$ ;  $\text{GMRotI}_{\text{PGA}}$  is the median of that distribution. This definition allows one to define an orientation-independent PGA, PGV, and PGV/PGA. All ground motion components are divided by the  $\text{GMRotI}_{\text{PGA}}$  and, subsequently, multiplied by the appropriate scaling factors so that  $\text{GMRotI}_{\text{PGA}}$  corresponds to the respective scaling factor. All of the waveforms, including their respective components, must be located in the same directory as the .ABF file.

The results of running a batch file are numerous .out files that are formatted text files, which are named in a similar fashion to the ground motion filenames. These .out files are located in the directory where the .stl files are located and provide two columns: the first corresponding to  $\text{GMRotI}_{\text{PGA}}$  and the second corresponding to the overturning probability. For each scaling factor, the horizontal ground motions are rotated by a random angle twice, and two separate simulations are undertaken. This results in overturning probabilities of either 0, 0.5, or 1. This convention has been chosen to reduce the number of computations and also to delineate a fragility that represents the uncertainty in the ground motion orientation relative to the object model orientation. Failure is determined via the condition that one of the free object components or blocks is located at a lower  $z$  position than the lowest fixed block, which is forced to move with the ground motion loaded. This definition of failure is conservative in the sense that noticeable rearrangements of the object components do not constitute failure but might be observable in the field. Such observations are easily quantified, however. Note that loading an .ABF file renders useless the ground motion start time, ground motion scaling factor, and time to cycle dialogs. Whether loading an .AT2 or an .ABF file should occur after the object model has been loaded.

Simulations are initiated with the  button and terminated with the  button. The simulation time dialog updates to show the current simulation time. The time step is calculated based on the block masses and stiffnesses, and should a ground motion recording be loaded, it is interpolated linearly to produce forcing amplitudes in conjunction with the simulation time step. The blocks that are not free are assigned the ground motion velocity at each time step and, as a result, are the forcing mechanisms for the free object component models.

## 2.4 COMPARISON WITH 3DEC

In order to demonstrate both the efficiency and accuracy of *Rigid*, a test model of a geode bouncing on a flat surface with gravity was simulated. The model geometry is shown in Figure 2.6. The identical model has been built in 3DEC with the identical physical parameters. The time steps have been set identically to 0.000314 sec per calculation cycle. The physical parameters include the following: the density =  $2600 \text{ kg/m}^3$ ,  $K_N = K_S = 10^{-9} \text{ N/m}$ , friction coefficient = 0, and damping = 0. The 3DEC model is composed of rigid blocks and the configuration has been set to dynamic. Both the 3DEC and *Rigid* models were run for 50 sec with the plot windows closed so that variations in plotting efficiency did not influence the results.

The *Rigid* model ran in ~11 sec while the identical 3DEC model ran in ~46 sec. Thus *Rigid* is ~4 times more efficient than 3DEC for this test case. In both cases, should the geode representation be perfect along with the *c-p* calculation, no rotational motion should occur. Accumulating errors and slight *c-p* imperfections will lead to some rotational motion, however. The accuracy of the *c-p* solution can be assessed by the number of impacts required for rotation to commence. For 3DEC, there is marked rotation after three impacts. Marked rotation does not occur in *Rigid*, however, until nine impacts have occurred. This demonstrates that the SLP approach used in *Rigid* is far superior to the *c-p* approach of Cundall [1988] in terms of accuracy. The 3DEC model also produced some very interesting results for the final geode configuration. Figure 2.6 shows that the initial geode representation has not been preserved in 3DEC after 50 sec of simulation time. This is due to the accumulation of round-off errors in the rotation logic used in 3DEC. As described above, *Rigid* takes special care to avoid such errors and this problem will not occur.

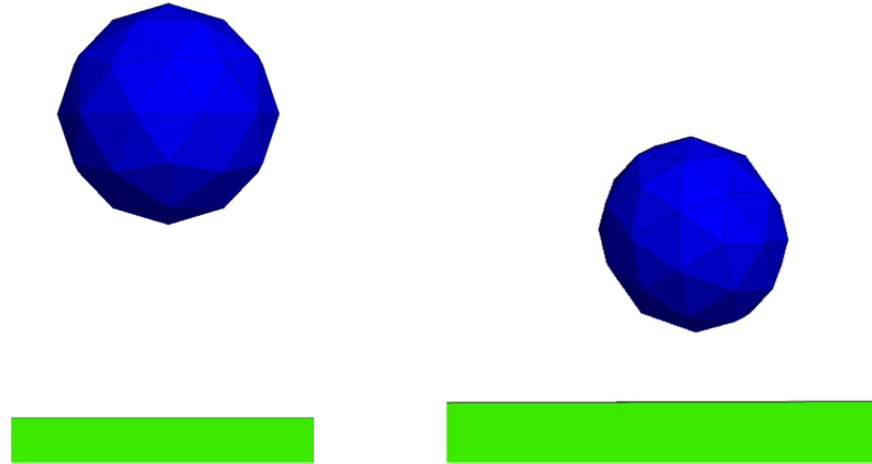


**Figure 2.6** A test model of a geode bouncing on a flat surface with gravity.



## 3 Numerical Analyses

### 3.1 OBJECTS SELECTED FOR ANALYSES

Since the Solitario Canyon Fault dominates the hazard in the vicinity of the designated repository at low probabilities, a total of nine geological features along the western slope of Yucca Mountain were selected for this fragility study. These rocks, listed in Table 3.1, are Class 2 and 3 features. These features are *in-place* freestanding rocks and freestanding or leaning rock stacks, which could provide constraints on unexceeded ground motions over the past 50–100 ka. Photographs of these features and their locations are shown in Figure 3.1. To obtain 3D fragilities using photogrammetry, relatively accurate shapes and sizes of these rocks have been determined. Figures 3.2 to 3.10 show photographs and shapes of these objects from several different angles.

**Table 3.1 List of the geological features studied.**

Geologic Feature	Approximate Location (degrees)	Class	Approximate Height (m)	Approximate Distance to Solitario Canyon Fault (km)
Fluffy	36.805, -116.477	3	1.1	0.58
Len	36.825, -116.469	3	2.7	0.81
Matt Cubed	36.835, -116.472	2	1.0	0.65
Nichole	36.855, -116.467	2	0.9	0.74
Pillow	36.809, -116.477	2	0.5	0.53
So. Yucca 2	36.800, -116.477	2	0.8	0.54
Sue	36.829, -116.471	2	0.8	0.64
Tripod	36.830, -116.471	3	1.8	0.68
Whitney	36.829, -116.471	3	1.3	0.65

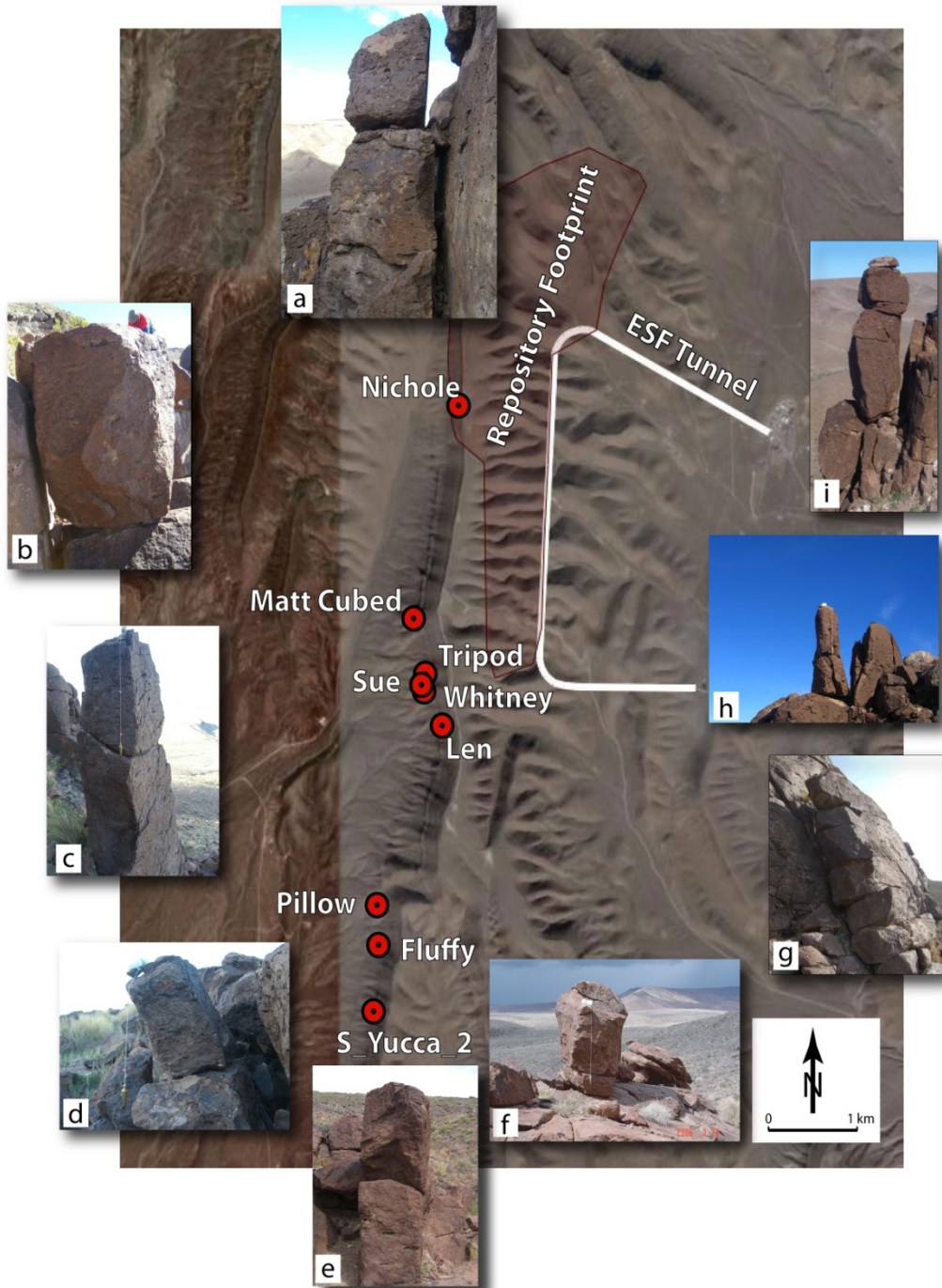


**Figure 3.1** Location map for the PBRs studied in this project. The photographs, counter-clockwise, are class 2 features (free-standing *in-place* single rocks): Nichole (a), Matt Cubed (b), Sue (c), Pillow (d), S\_Yucca\_2 (e), and Fluffy (f), and class 3 features (*in-place* rock stacks): Len (g), Whitney (h), and Tripod (i).

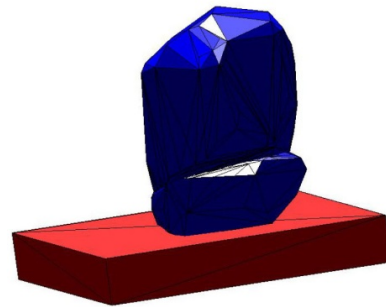
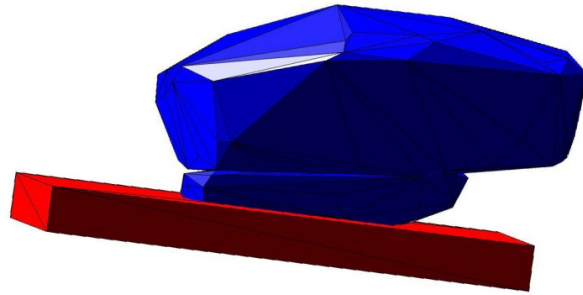
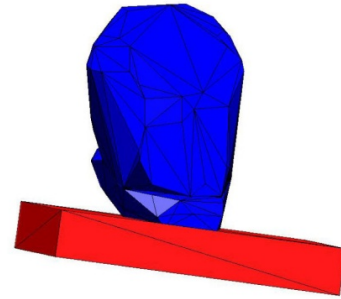


**Figure 3.2** Fluffy is a Class 3 feature that is located at a distance of about 0.58 km from the Solitario Canyon Fault. It is composed of two separate pieces that rest on a relatively flat ground surface. The combine height is about 1.1 m. Photographs taken from different angles are shown next to the corresponding orientations of the 3D shape used in the numerical simulations.

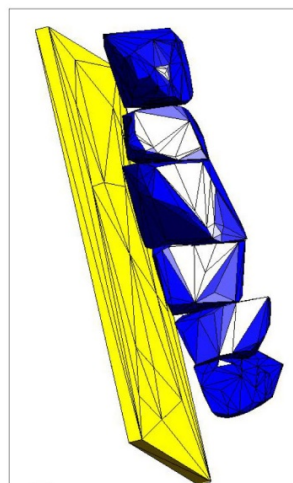
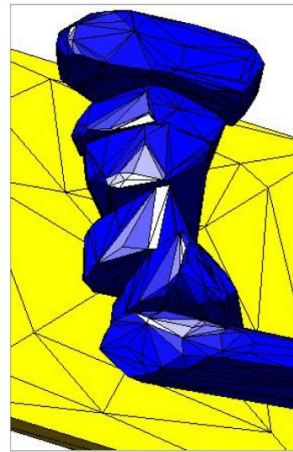
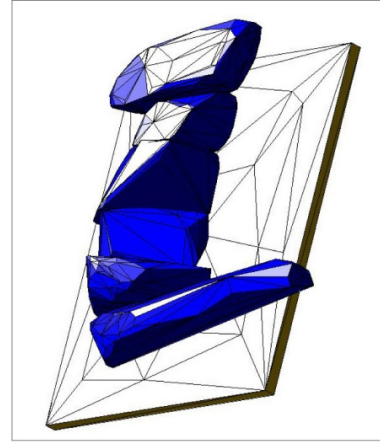


**Figure 3.3** Len is a Class 3 stack of rocks that is located in the middle ledge of the Western slope of Yucca Mountain at a distance of about 0.81 km from the Solitario Canyon Fault. The stack is about 2.7 m high and is composed of several separate rocks that lean eastward, against the mountain side. Only the top 5 pieces have been modeled in this study. Photographs taken from different angles are shown next to the corresponding orientations of the 3D shape used in the numerical simulations.

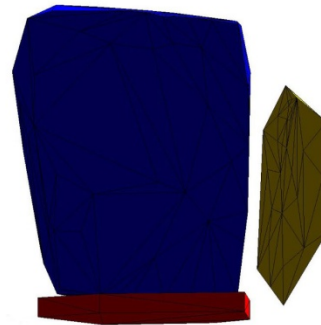
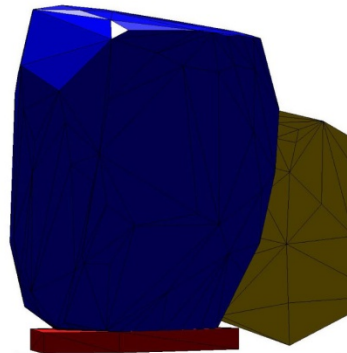
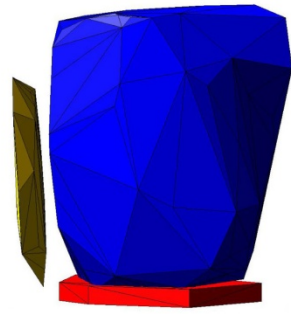


**Figure 3.4** Matt Cubed is a Class 2 rock that is located in the middle ledge of the Western slope of Yucca Mountain at a distance of about 0.65 km from the Solitario Canyon Fault. It is a 1-m-high rectangular-shaped rock that sits against the mountain face. Photographs taken from different angles are shown next to the corresponding orientations of the 3D shape used in the numerical simulations.

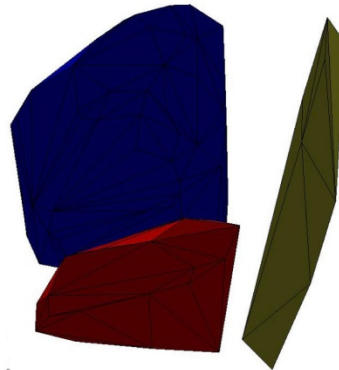
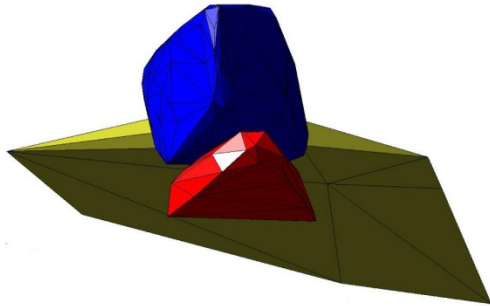
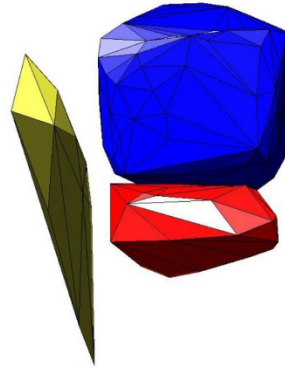


**Figure 3.5** Nichole is a Class 2 rock that is located in the middle ledge of the western slope of Yucca Mountain at a distance of about 0.74 km from the Solitario Canyon Fault. This the northernmost rock studied here. Photographs taken from different angles are shown next to the corresponding orientations of the 3D shape used in the numerical simulations.

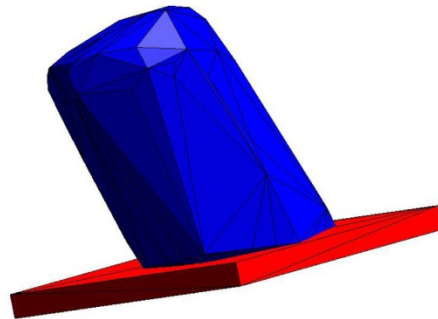
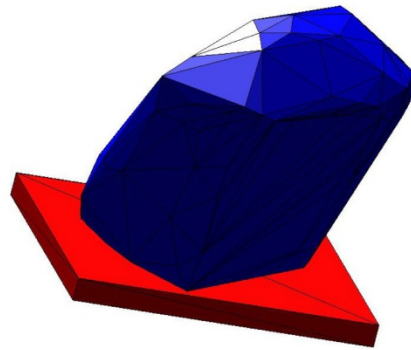
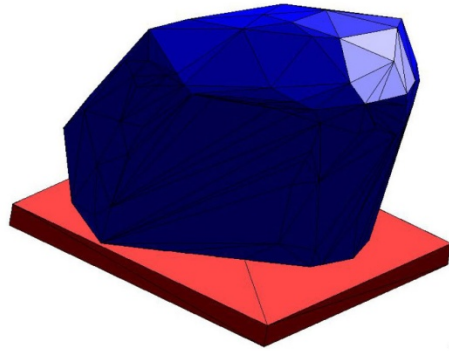


**Figure 3.6** Pillow is a Class 2 rock that is located near the foot of Yucca Mountain. It has a height of about 0.5 m and is at about 0.53 km from the Solitario Canyon Fault. Photographs taken from different angles are shown next to the corresponding orientations of the 3D shape used in the numerical simulations.

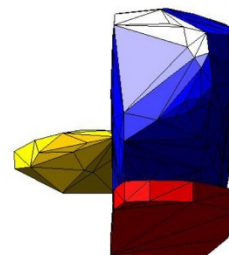
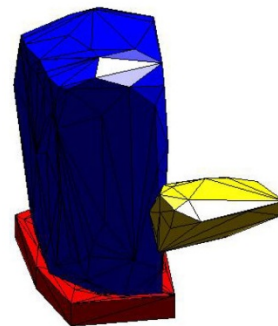
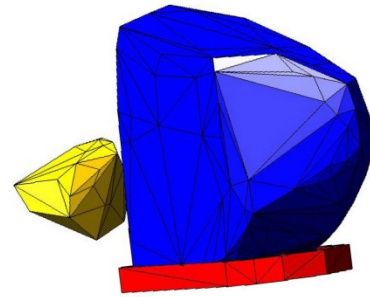


**Figure 3.7** S-Yucca\_2 is a Class 2 rock that is located in the middle ledge of the western slope of Yucca Mountain at a distance of about 0.54 km from the Solitario Canyon Fault. This is the southernmost rock used in this study. This is a fairly fragile rock that could topple in almost every direction, except for a small rock at one corner that restricts its motion. Photographs taken from different angles are shown next to the corresponding orientations of the 3D shape used in the numerical simulations.

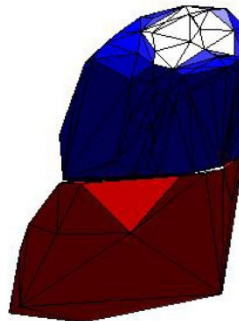
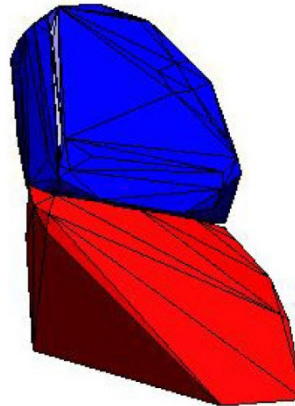
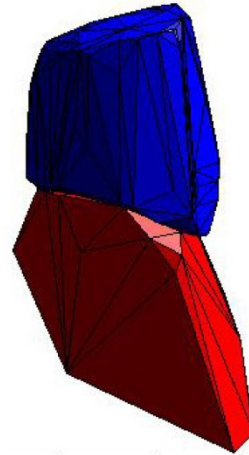


**Figure 3.8**

**Sue is a Class 2 rock that is located in the middle ledge of the western slope of Yucca Mountain at a distance of about 0.64 km from the Solitario Canyon Fault. Although this is not very fragile, its location on a high pedestal suggests of a very long age. Photographs taken from different angles are shown next to the corresponding orientations of the 3D shape used in the numerical simulations.**

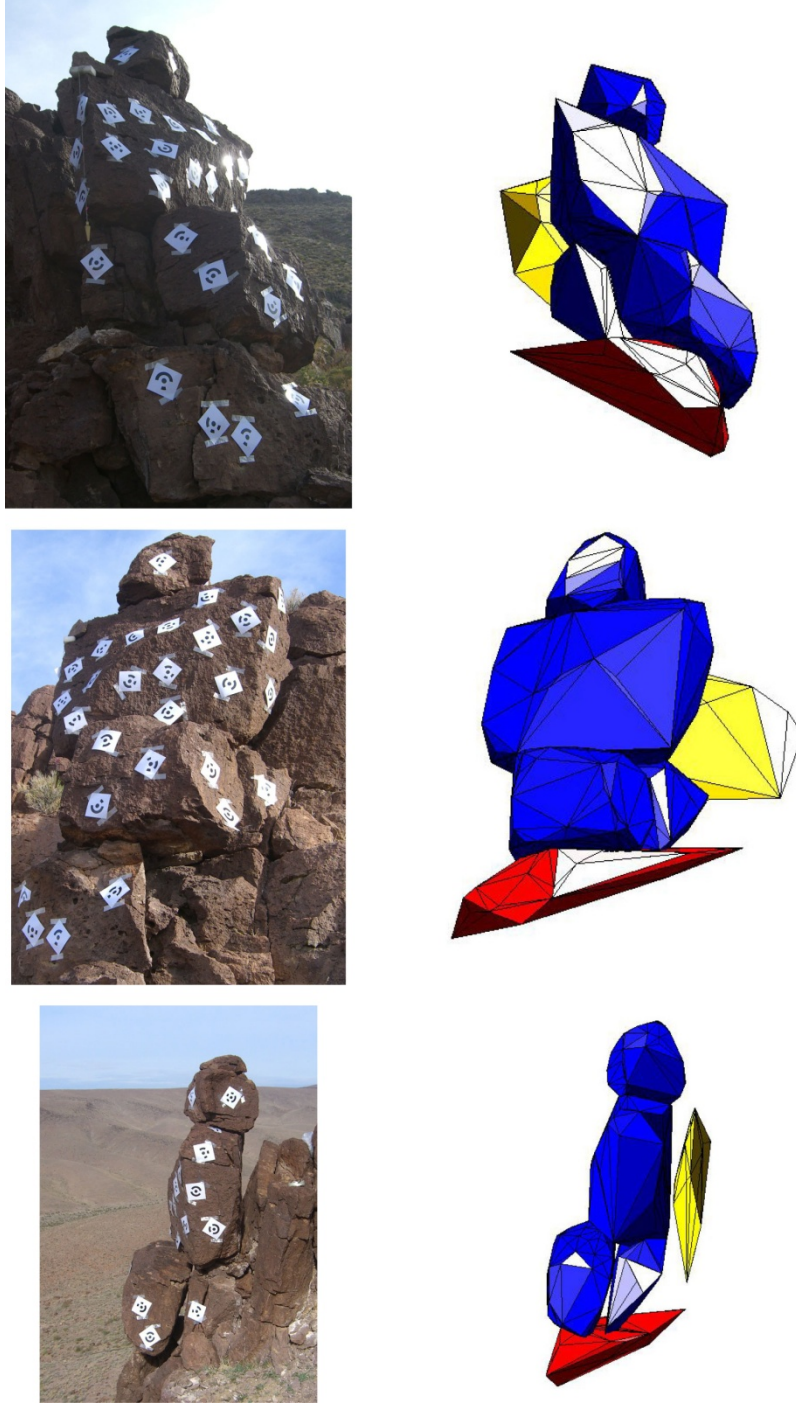


**Figure 3.9** Tripod is a Class 3 stack of rocks that is located in the middle ledge of the Western slope of Yucca Mountain at a distance of about 0.68 km from the Solitario Canyon Fault. This very fragile stack is about 1.8 m high and is composed of four rocks. It rests on a pedestal that is also unstable. Photographs taken from different angles are shown next to the corresponding orientations of the 3D shape used in the numerical simulations.

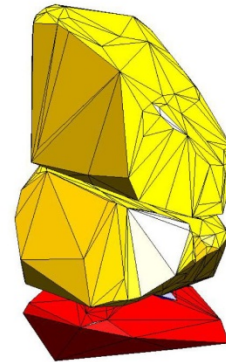
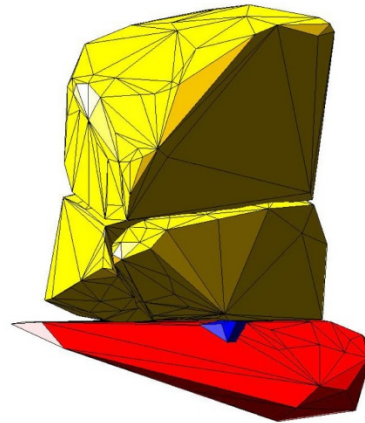
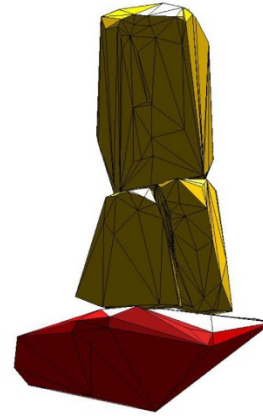


**Figure 3.10** Whitney is a Class 3 stack of rocks that is located in the middle ledge of the Western slope of Yucca Mountain at a distance of about 0.65 km from the Solitario Canyon Fault. This very fragile stack is about 1.3 m high and is composed of three rocks. It rests on a sloping pedestal. A small rock, wedged between one of the rocks and the pedestal prevents the stack from collapse. Photographs taken from different angles are shown next to the corresponding orientations of the 3D shape used in the numerical simulations. The wedge is shown in blue color.

### 3.2 COMPARISON WITH ANDREWS ET AL. [2007] GROUND MOTIONS

What types of ground motions might one expect from an earthquake on the Solitario Canyon Fault, which lies a few 100 m to the west of the repository? Andrews et al. [2007] undertook 2D simulations of normal faulting earthquakes on the Solitario Canyon Fault to answer this question. They estimated surface slip from trenching studies and constructed subshear and supershear rupture models that produced these surface offsets. In particular, they developed a fault displacement likelihood model as follows: 0.1 weight to no earthquake in the past 77 ka, 0.2 weight to 0.5 m slip in an earthquake within the past 77 ka, 0.3 weight 1.3 m slip in an earthquake within the past 77 ka, and 0.4 weight to 2.7 m of slip in an earthquake within the past 77 ka. This fault lies at the base of Yucca Mountain, and the objects selected for these analyses lie within 10 sec to 100 sec of meters of the surface outcrop of this fault.

Andrews [personal communication 2009] provided ground motions calculated at the free surface for these analyses calculated as part of the Andrews [2007] effort. Those waveforms have been filtered to 6 Hz, the maximum frequency resolved by the simulations and converted to the PEER format described above. The normal faulting events correspond to a mode II rupture where rupture travels purely in the up-dip direction; as a result, there are no transverse ground motions. The Yucca Mountain objects have been oriented relative to north and, as a result, are exposed to E-W and vertical ground motions. Table 3.2 presents the results of overturning analyses for the 0.5 m, 1.3 m, and 2.7 m offsets for both subshear and supershear scenarios. Neither of the 0.5-m scenarios overturns any of the objects investigated. The 1.3-m-subshear event overturns two of the objects, and the 2.7-m-subshear event overturns five of the nine objects investigated. The 1.3-m-supershear event, on the other hand, overturns zero objects and the 2.7-m-supershear overturns three of the objects. Should all of these objects have resided in their current positions for the past 77 ka, they would indicate that the 2.7-m slip scenarios as modeled by Andrews et al. [2007] produce unrealistically high amplitude ground motions. In fact, the 1.3-m subshear scenario is also inconsistent with 77 ka ages for these Yucca Mountain features.

**Table 3.2 Overturning analyses of geological features listed in Table 3.1 subjected to both subshear and supershear scenarios of Andrews et al. [2007].**

Rock Height	Subshear			Supershear		
	0.5 m	1.3 m	2.7 m	0.5 m	1.3 m	2.7 m
Fluffy	0	0	0	0	0	0
Len	0	0	0	0	0	0
Matt Cubed	0	1	1	0	0	1
Nichole	0	0	1	0	0	0
Pillow	0	0	1	0	0	0
S_Yucca_2	0	0	0	0	0	0
Sue	0	0	0	0	0	0
Tripod	0	0	1	0	0	1
Whitney	0	1	1	0	0	1

### 3.3 COMPARISON WITH WONG WAVEFORMS

Wong [2004] documented the creation of waveforms for both pre-closure and post-closure site assessment for the Yucca Mountain waste repository. Ground motions were generated based on the Yucca Mountain PSHA [Stepp et al. 2001] via random vibration theory for Point A, a reference rock outcrop site. The Point A ground motions were modified by a site response model based on a one-dimensional (1D) equivalent-linear representation of the local site velocities to produce ground motions at Point B, a rock site in the waste emplacement level. The spectra of the Point B ground motions have been conditioned on Point A spectra so that they are not drastically dissimilar in spectral shape to a rock site on the free surface. Point B lies ~ 300 m below the sites of the fragile geological features investigated in this study.

As shown in Figures 6.3–151 and 6.3–154 of Wong [2004] for the  $10^{-4}$  annual exceedance frequencies, horizontal PGA at 300 m depth is ~ 45% of PGA at the surface (Point C) and horizontal PGV at 300 m depth is ~ 60% of PGV at the surface. Thus the horizontal PGAs and PGVs of the Point B ground motions underestimate the free surface ground motions. Seventeen sets of ground motion time histories were created in Wong [2004] for post-closure analyses; the ground motions are for annual exceedance frequencies of  $10^{-5}$  and  $10^{-6}$ . The original Excel files of the ground motion time histories contain an error in set 4 and, as a result, set 4 has been removed from these analyses; thus 16 sets were analyzed. Batch processing was undertaken for each of the fragile Yucca Mountain features as described above; i.e., the two horizontal components were randomly rotated twice, and each object model was exposed to both of the rotated sets of ground motions. Thus the overturning probability may be either 0, 0.5, or 1.

The results of these analyses are shown in Table 3.3. The following  $10^{-5}$  sets overturn all of the object models during at least one of the two tests: 2, 3, 5, 6, 7, 8, 9, 11, 12, and 13. Set 15 is the only set that did not overturn any of the object models. Each of the remaining  $10^{-5}$  ground motions for Point B were inconsistent with at least two of the fragile features on Yucca Mountain. As mentioned above, one might multiply these Point B waveforms by a factor of two to correspond to the locations of the fragile features investigated in this work. Table 3.4 shows the results for the simulations using  $10^{-5}$  exceedance frequency ground motions multiplied by a factor of two. In this case, none of the sets result in survival of all of the object models. Table 3.5 demonstrates the results for the  $10^{-6}$  annual exceedance probability waveforms for Point B. All of the  $10^{-6}$  ground motion sets produce overturning of the object models in at least one of the two simulations. The Yucca Mountain features may not have survived for the past  $1e5$  years, though.

**Table 3.3 Overturning results for the 10<sup>-5</sup> exceedance ground motions at Point B.**

	Set																
	1	2	3	5	6	7	8	9	10	11	12	13	14	15	16	17	
GMRotl_PGA (g)	2.481	2.433	4.592	3.785	1.895	0.582	1.879	2.214	3.001	1.017	2.241	1.055	0.380	0.128	0.817	0.385	
GMRotl_PGV (cm/sec)	86.306	127.498	175.773	131.229	83.301	94.871	133.305	226.023	67.055	106.751	86.384	98.852	70.226	70.834	82.408	93.051	
Ratio (sec)	0.035	0.053	0.039	0.035	0.045	0.166	0.072	0.104	0.023	0.107	0.039	0.096	0.188	0.566	0.103	0.247	
Fluffy	1	1	1	1	0.5	1	1	1	0	1	1	1	0	0	1	0	
Len	1	1	1	0.5	1	0.5	0.5	1	0.5	1	1	1	0	0	0	0	
Matt Cubed	1	1	1	1	1	1	1	1	1	1	1	1	1	0	1	1	
Nichole	1	1	1	1	1	1	1	1	1	1	1	1	0	0	1	0	
Pillow	1	1	1	1	1	1	1	1	1	1	1	1	0.5	0	1	1	
S_Yucca_2	0	1	1	1	1	0.5	0.5	1	0.5	1	0.5	1	0	0	1	0	
Sue	1	1	1	1	1	1	1	1	1	1	1	1	0	0	1	0	
Tripod	1	1	1	1	1	1	1	1	1	1	1	1	1	0	1	1	
Whitney	1	1	1	1	1	1	1	1	1	1	1	1	0	0	1	1	

**Table 3.4 Overturning results for the 10<sup>-5</sup> exceedance ground motions at Point B multiplied by a factor of two.**

	Set																
	1	2	3	5	6	7	8	9	10	11	12	13	14	15	16	17	
GMRotl_PGA (g)	4.962	4.867	9.185	7.570	3.789	1.164	3.759	4.429	6.002	2.034	4.482	2.111	0.760	0.255	1.634	0.770	
GMRotl_PGV (cm/sec)	172.612	254.995	351.546	262.458	166.601	189.741	266.610	452.046	134.111	213.502	172.767	197.705	140.451	141.669	164.816	186.103	
Ratio (sec)	0.035	0.053	0.039	0.035	0.045	0.166	0.072	0.104	0.023	0.107	0.039	0.096	0.188	0.566	0.103	0.247	
Fluffy	1	1	1	1	1	1	1	1	1	1	1	1	1	0	0.5	1	
Len	1	1	1	1	1	1	1	1	1	1	1	1	0.5	0	1	1	
Matt Cubed	1	1	1	1	1	1	1	1	1	1	1	1	1	1	1	1	
Nichole	1	1	1	1	1	1	1	1	1	1	1	1	1	0	1	1	
Pillow	1	1	1	1	1	1	1	1	1	1	1	1	0.5	0	1	1	
S_Yucca_2	1	1	1	1	1	1	1	1	0.5	1	1	1	0.5	0	1	1	
Sue	1	1	1	1	1	1	1	1	1	1	1	1	0.5	0	1	1	
Tripod	1	1	1	1	1	1	1	1	1	1	1	1	1	1	1	1	
Whitney	1	1	1	1	1	1	1	1	1	1	1	1	1	0.5	1	1	

**Table 3.5 Results for the 10<sup>-6</sup> annual exceedance probability waveforms for Point B.**

	Set																
	1	2	3	5	6	7	8	9	10	11	12	13	14	15	16	17	
GMRotI_PGA (g)	6.705	6.049	13.093	8.235	6.323	2.337	5.557	6.100	8.178	2.701	2.241	3.537	2.087	0.845	2.599	1.180	
GMRotI_PGV (cm/sec)	209.177	285.423	422.824	235.141	181.324	239.426	342.913	521.421	163.083	233.454	86.384	272.430	181.234	190.802	196.571	190.800	
Ratio (sec)	0.032	0.048	0.033	0.029	0.029	0.105	0.063	0.087	0.020	0.088	0.039	0.079	0.089	0.230	0.077	0.165	
Fluffy	1	1	1	1	1	1	1	1	1	1	1	1	1	1	1	1	
Len	1	1	1	1	1	1	1	1	1	1	1	1	1	1	1	1	
Matt Cubed	1	1	1	1	1	1	1	1	1	1	1	1	1	1	1	1	
Nichole	1	1	1	1	1	1	1	1	1	1	1	1	1	1	1	1	
Pillow	1	1	1	1	1	1	1	1	1	1	1	1	1	1	1	1	
S_Yucca_2	1	1	1	1	1	1	1	1	1	1	0.5	1	1	1	1	1	
Sue	1	1	1	1	1	1	1	1	1	1	1	1	1	1	1	1	
Tripod	1	1	1	1	1	1	1	1	1	1	1	1	1	1	1	1	
Whitney	1	1	1	1	1	1	1	1	1	1	1	1	1	1	1	1	

How do these Point B ground motion amplitudes compare with the  $10^{-4}$  annual exceedance frequency ground motion amplitudes? As shown in Stepp et al. [2001], the median the  $10^{-5}$  ground motion amplitudes (both PGA and  $S_A$  at 1 Hz, which is a proxy for PGV) are roughly a factor of two greater than the  $10^{-4}$  ground motion amplitudes. Thus, the  $10^{-5}$  ground motions at Point B can be seen as a rough proxy for the  $10^{-4}$  ground motions expected on the flanks of Yucca Mountain in terms of the parameters important for overturning the fragile geological features. This suggests that  $10^{-4}$  waveforms produced in a similar manner would be broadly inconsistent with the objects that exist on Yucca Mountain investigated in this report.

### 3.4 WAVEFORMS SELECTED FOR FRAGILITY ANALYSES

Purvance et al. [2008] viewed fragility delineation as a numerical experiment with the object models and waveforms being viewed as inputs to the process. Determining which waveforms are the best for fragility delineation depends strongly on the waveform characteristics that lead directly to object failure. Purvance et al. [2008] determined that PGA and PGV/PGA (which is strongly correlated with the duration of the largest acceleration pulse) are the primary waveform characteristics leading to failure. As discussed in Purvance et al. [2008], other factors, such as the duration of strong shaking and the envelope shape of the input waveform, are much less important. As the specific objects investigated in this effort are located on Yucca Mountain, one would ideally use waveforms for fragility calculations for earthquake magnitude-distance pairs similar to Yucca Mountain expectations (e.g., recordings of normal faulting earthquakes with magnitudes  $M > 6.0$  recorded at distances  $D < 100$  m from the fault). Unfortunately no recordings of events like this exist.

Using guidance from Purvance et al. [2008], the decision was made to select waveforms from the PEER strong-motion database (<http://peer.berkeley.edu/smcat/data.html>) with  $M \geq 6.0$  that were recorded at fault distances less than 10 km. Recordings that demonstrated significant effects from very low velocities near the surface were removed. Upon inspection of the remaining waveforms, it was determined that few with large PGV/PGA values were included in this sample. Thus a few recordings at greater distances of  $M \geq 6.0$  were added. In addition, time windows were selected to diminish the computational efforts where the times to start the computations were set as the S-wave arrivals. On average, the waveform durations simulated are 15 sec and range from  $\sim 10$  sec to  $\sim 30$  sec. Table 3.6 includes a list of earthquake names, earthquake years, earthquake magnitudes, waveform names, simulation start times, end times,  $\text{GMRotI}_{\text{PGA}}$  (g),  $\text{GMRotI}_{\text{PGV}}$  (cm/sec), and  $\text{GMRotI}_{\text{PGV}}/\text{GMRotI}_{\text{PGA}}$  (sec). One hundred and fifty-four separate earthquake recordings were used for fragility estimation in the current effort.

**Table 3.6 List of waveforms selected for fragility analyses.**

<b>Earthquake Name</b>	<b>Year</b>	<b>Mag</b>	<b>File Name</b>	<b>Start time (s)</b>	<b>End Time (s)</b>	<b>GMRotIPGA (g)</b>	<b>GMRotIPGV (cm/s)</b>	<b>GMRotIPGV/GMRotIPGA (s)</b>
St Elias, Alaska	1979	7.54	059v2-X.AT2	13.7903	40.3341	0.06955	34.2635	0.50236
Northridge-01	1994	6.69	0637-X.AT2	2.477	12.0392	0.78317	72.6563	0.094602
Northridge-01	1994	6.69	0655-X.AT2	1.97	9.0207	0.74867	74.255	0.10114
Hector Mine	1999	7.13	0997-X.AT2	24.5968	48.4677	0.059871	20.437	0.34808
Duzce, Turkey	1999	7.14	1058-X.AT2	11.7512	27.6959	0.091117	13.2211	0.14796
Duzce, Turkey	1999	7.14	1059-X.AT2	13.4274	30.2247	0.13615	12.4816	0.093482
Duzce, Turkey	1999	7.14	1062-X.AT2	14.4643	30.121	0.20127	13.4749	0.068271
Duzce, Turkey	1999	7.14	375-X.AT2	14.3606	20.7892	0.70435	28.0423	0.040598
Northridge-01	1994	6.69	5108-X.AT2	1.5899	13.4793	0.25271	16.9602	0.068436
Duzce, Turkey	1999	7.14	531-X.AT2	14.1532	22.7592	0.1429	13.4723	0.096134
Irpinia, Italy-01	1980	6.90	A_BAG-X.AT2	2.9032	12.6728	0.16182	26.3616	0.16612
Managua, Nicaragua-01	1972	6.24	A_MAN-X.AT2	1.4171	11.5092	0.39406	25.3058	0.065484
Irpinia, Italy-01	1980	6.90	A_STU-X.AT2	3.5484	14.1475	0.29506	43.5694	0.15058
Chalfant Valley-02	1986	6.19	A_ZAK-X.AT2	2.9032	9.0783	0.41801	41.125	0.10032
Chi-Chi, Taiwan	1999	7.62	ALS-X.AT2	16.5207	32.8341	0.17455	29.2926	0.17112
Morgan Hill	1984	6.19	AND-X.AT2	2.523	7.8456	0.34873	29.2083	0.085406
Northridge-01	1994	6.69	ARL-X.AT2	2.0737	11.7512	0.32156	30.5239	0.096795
Irpinia, Italy-02	1980	6.20	B_CTR-X.AT2	2.8226	15.4954	0.17718	24.3006	0.13986
Loma Prieta	1989	6.93	BRN-X.AT2	9.159	17.3848	0.51365	48.6372	0.096557
Parkfield	1966	6.19	C05-X.AT2	4.303	11.7684	0.37507	23.0186	0.062582
N. Palm Springs	1986	6.06	CAB-X.AT2	2.1025	13.6809	0.21501	11.1151	0.052714
Loma Prieta	1989	6.93	CAP-X.AT2	3.4562	16.8203	0.47989	34.0549	0.072363
Northridge-01	1994	6.69	CHL-X.AT2	2.7823	15.2823	0.21007	22.6865	0.11013
Chi-Chi, Taiwan	1999	7.62	CHY006-X.AT2	24.712	51.3249	0.35504	51.9555	0.14922
Chi-Chi, Taiwan	1999	7.62	CHY024-X.AT2	27.8917	49.0438	0.23474	51.306	0.22288
Chi-Chi, Taiwan	1999	7.62	CHY028-X.AT2	32.6613	43.8594	0.76276	73.5647	0.098347
Chi-Chi, Taiwan	1999	7.62	CHY074-X.AT2	4.2857	18.1106	0.32431	36.5895	0.11505
Chi-Chi, Taiwan	1999	7.62	CHY080-X.AT2	30.5876	42.2005	0.81521	103.7374	0.12976
Chi-Chi, Taiwan	1999	7.62	CHY101-X.AT2	26.6475	50.9101	0.38839	90.2213	0.23687
Chi-Chi, Taiwan	1999	7.62	CHY104-X.AT2	35.4263	68.9516	0.17507	54.1282	0.31528
Loma Prieta	1989	6.93	CLS-X.AT2	1.6129	10.553	0.52146	47.9348	0.093736
Northridge-01	1994	6.69	CNP-X.AT2	1.6993	11.9528	0.36731	47.0399	0.13059

Earthquake Name	Year	Mag	File Name	Start time (s)	End Time (s)	GMRotIPGA (g)	GMRotIPGV (cm/s)	GMRotIPGV/GMRotIPGA (s)
Cape Mendocino	1992	7.01	CPM-X.AT2	2.3157	7.1544	1.2978	83.7232	0.065785
Morgan Hill	1984	6.19	CYC-X.AT2	2.523	6.5323	0.9349	65.4526	0.07139
Tabas, Iran	1978	7.35	DAY-X.AT2	2.3906	14.2569	0.34747	26.357	0.077351
Dinar, Turkey	1995	6.40	DIN-X.AT2	2.2465	19.2512	0.30564	32.5978	0.10876
Duzce, Turkey	1999	7.14	DZC-X.AT2	1.9009	18.076	0.42803	69.6137	0.16584
Loma Prieta	1989	6.93	G01-X.AT2	2.6267	8.341	0.43462	32.4138	0.07605
Morgan Hill	1984	6.19	G06-X.AT2	0.72581	12.1313	0.26901	23.2274	0.088045
Gazli, USSR	1976	6.80	GAZ-X.AT2	4.6244	13.0438	0.6456	64.9497	0.10259
Kocaeli, Turkey	1999	7.51	GBZ-X.AT2	4.0438	14.7581	0.18141	38.2092	0.21478
Loma Prieta	1989	6.93	GIL-X.AT2	1.9816	7.9724	0.3546	26.9339	0.077453
Imperial Valley-06	1979	6.53	H_AEP-X.AT2	1.4516	10.0783	0.32055	32.25	0.10259
Imperial Valley-06	1979	6.53	H_AGR-X.AT2	2.4539	13.5829	0.2896	33.73	0.11877
Imperial Valley-06	1979	6.53	H_BCR-X.AT2	2.2581	12.9493	0.67066	49.5524	0.075343
Imperial Valley-06	1979	6.53	H_BRA-X.AT2	5.2995	18.1106	0.18493	37.467	0.2066
Imperial Valley-06	1979	6.53	H_E04-X.AT2	2.9032	16.2673	0.40151	69.4198	0.1763
Imperial Valley-06	1979	6.53	H_E05-X.AT2	3.8249	18.5714	0.44159	71.7188	0.16561
Imperial Valley-06	1979	6.53	H_E06-X.AT2	4.3779	15.3456	0.40816	83.8778	0.20956
Imperial Valley-06	1979	6.53	H_E07-X.AT2	3.5484	16.7281	0.40741	78.0789	0.19543
Imperial Valley-06	1979	6.53	H_E08-X.AT2	3.9171	15.6221	0.52346	52.658	0.10258
Imperial Valley-06	1979	6.53	H_E10-X.AT2	3.8249	20.5991	0.19893	46.1766	0.2367
Imperial Valley-06	1979	6.53	H_ECC-X.AT2	4.7465	24.5622	0.20942	48.9909	0.23855
Imperial Valley-06	1979	6.53	H_EDA-X.AT2	3.8249	15.53	0.42358	56.0961	0.13504
Imperial Valley-06	1979	6.53	H_EMO-X.AT2	3.0876	12.3041	0.3039	70.4562	0.23641
Imperial Valley-06	1979	6.53	H_HVP-X.AT2	3.0876	19.4931	0.23433	47.4695	0.20657
Coalinga-01	1983	6.36	H_PVB-X.AT2	3.2719	15.8065	0.31718	26.5834	0.085465
Coalinga-01	1983	6.36	H_PVY-X.AT2	3.1797	13.5023	0.5526	44.9806	0.083002
Morgan Hill	1984	6.19	HVR-X.AT2	1.1521	15.2535	0.21927	24.9453	0.11601
Mammoth Lakes-01	1980	6.06	I_CVK-X.AT2	3.629	12.5461	0.43018	23.3692	0.055395
Mammoth Lakes-01	1980	6.06	I_MLS-X.AT2	4.8041	15.3802	0.28465	13.8218	0.049514
Kocaeli, Turkey	1999	7.51	IZT-X.AT2	1.7627	10.1959	0.20284	26.7966	0.13471
Northridge-01	1994	6.69	JEN-X.AT2	1.4171	9.7811	0.74874	73.9858	0.10076
Northridge-01	1994	6.69	KAT-X.AT2	2.5634	10.5127	0.75482	42.1136	0.056893
Kobe, Japan	1995	6.90	KJM-X.AT2	6.6244	19.0668	0.70427	75.5928	0.10945
Northridge-01	1994	6.69	LA0-X.AT2	7.8226	17.6613	0.32685	30.0516	0.093756
Landers	1992	7.28	LCN-X.AT2	6.1636	18.03	0.73687	96.2517	0.1332

Earthquake Name	Year	Mag	File Name	Start time (s)	End Time (s)	GMRotIPGA (g)	GMRotIPGV (cm/s)	GMRotIPGV/GMRotIPGA (s)
Northridge-01	1994	6.69	LDM-X.AT2	2.2465	10.265	0.45563	56.3697	0.12616
Loma Prieta	1989	6.93	lex-X.AT2	2.0161	9.5968	0.45331	72.7464	0.16364
Loma Prieta	1989	6.93	LGP-X.AT2	7.0853	16.3479	0.75255	79.552	0.10779
Northridge-01	1994	6.69	MUL-X.AT2	2.4539	13.7903	0.46892	57.1872	0.12436
N. Palm Springs	1986	6.06	MVH-X.AT2	1.1809	10.5127	0.20945	34.8222	0.16953
Kobe, Japan	1995	6.90	NIS-X.AT2	4.1993	19.7523	0.48596	36.0463	0.075638
N. Palm Springs	1986	6.06	NPS-X.AT2	2.0449	7.8053	0.60969	49.9458	0.083536
Chi-Chi, Taiwan	1999	7.62	NSY-X.AT2	20.9447	44.447	0.13334	43.7885	0.33488
Northridge-01	1994	6.69	NWH-X.AT2	3.5484	11.2903	0.67077	83.7104	0.12726
Northridge-01	1994	6.69	PAC-X.AT2	2.6037	8.6406	0.40656	35.2143	0.088322
Northridge-01	1994	6.69	PAR-X.AT2	3.5426	11.0311	0.50295	57.5833	0.11675
Cape Mendocino	1992	7.01	PET-X.AT2	1.7051	14.0553	0.59271	69.1846	0.11903
Northridge-01	1994	6.69	PKC-X.AT2	2.2581	13.7788	0.35523	42.0401	0.12068
Denali, Alaska	2002	7.90	ps10-X.AT2	23.4798	42.7863	0.32258	98.4491	0.31121
San Fernando	1971	6.61	PUL-X.AT2	1.6071	11.8721	1.1575	77.9543	0.068676
Cape Mendocino	1992	7.01	RIO-X.AT2	2.9032	11.5668	0.44508	45.2535	0.10368
Northridge-01	1994	6.69	RRS-X.AT2	1.1751	7.3502	0.65971	109.1774	0.16876
Nahanni, Canada	1985	6.76	S1-X.AT2	0.9375	11.0988	1.0146	44.0861	0.04431
Nahanni, Canada	1985	6.76	S3-X.AT2	2.3952	12.6855	0.15341	5.011	0.033309
Northridge-01	1994	6.69	SCE-X.AT2	1.4677	11.4677	0.6461	90.6825	0.14312
Northridge-01	1994	6.69	SCS-X.AT2	1.4355	13.7258	0.71133	108.0239	0.15486
Loma Prieta	1989	6.93	STG-X.AT2	3.7581	13.2419	0.38733	45.9478	0.12097
Northridge-01	1994	6.69	SYL-X.AT2	2.3387	12.4032	0.68262	94.3706	0.14097
Tabas, Iran	1978	7.35	TAB-X.AT2	3.9375	16.1875	0.80723	108.5115	0.13707
Kobe, Japan	1995	6.90	TAK-X.AT2	1.506	14.9698	0.63369	116.5837	0.1876
Chi-Chi, Taiwan	1999	7.62	TAP047-X.AT2	33.3508	61.9476	0.053143	16.6814	0.32009
Northridge-01	1994	6.69	TAR-X.AT2	2.6613	13.5645	1.5542	90.1388	0.05914
Kobe, Japan	1995	6.90	TAZ-X.AT2	3.1391	13.7359	0.69352	75.7114	0.11132
Chi-Chi, Taiwan	1999	7.62	TCU007-X.AT2	33.6411	60.2056	0.065533	20.5642	0.31999
Chi-Chi, Taiwan	1999	7.62	TCU011-X.AT2	8.0867	24.994	0.069587	23.2509	0.34072
Chi-Chi, Taiwan	1999	7.62	TCU015-X.AT2	42.7137	62.746	0.11414	37.7943	0.33765
Chi-Chi, Taiwan	1999	7.62	TCU017-X.AT2	39.5202	58.8266	0.096428	35.0981	0.37116
Chi-Chi, Taiwan	1999	7.62	TCU018-X.AT2	32.6774	49.7742	0.055807	26.6742	0.4874
Chi-Chi, Taiwan	1999	7.62	TCU026-X.AT2	35.4556	56.6492	0.098956	30.9088	0.31851
Chi-Chi, Taiwan	1999	7.62	TCU031-X.AT2	40.3185	62.3831	0.12577	49.0493	0.39768

Earthquake Name	Year	Mag	File Name	Start time (s)	End Time (s)	GMRotIPGA (g)	GMRotIPGV (cm/s)	GMRotIPGV/GMRotIPGA (s)
Chi-Chi, Taiwan	1999	7.62	TCU036-X.AT2	38.8669	62.0927	0.13288	54.0154	0.41453
Chi-Chi, Taiwan	1999	7.62	TCU038-X.AT2	43.0766	61.7298	0.14991	45.4452	0.30913
Chi-Chi, Taiwan	1999	7.62	TCU039-X.AT2	38.3589	62.9637	0.18198	55.4653	0.3108
Chi-Chi, Taiwan	1999	7.62	TCU040-X.AT2	37.4153	57.5202	0.12737	49.6296	0.39734
Chi-Chi, Taiwan	1999	7.62	TCU049-X.AT2	26.6734	50.1895	0.27221	53.9643	0.20215
Chi-Chi, Taiwan	1999	7.62	TCU050-X.AT2	28.2702	55.0524	0.13592	39.2572	0.29451
Chi-Chi, Taiwan	1999	7.62	TCU051-X.AT2	28.996	51.2056	0.21179	43.251	0.20825
Chi-Chi, Taiwan	1999	7.62	TCU052-X.AT2	30.375	47.9395	0.34676	129.1271	0.37972
Chi-Chi, Taiwan	1999	7.62	TCU053-X.AT2	27.1089	57.7379	0.18188	44.558	0.24982
Chi-Chi, Taiwan	1999	7.62	TCU054-X.AT2	25.5121	56.4315	0.16859	48.6444	0.29422
Chi-Chi, Taiwan	1999	7.62	TCU057-X.AT2	24.7137	53.1653	0.10916	36.3303	0.33938
Chi-Chi, Taiwan	1999	7.62	TCU059-X.AT2	27.7621	57.8105	0.1588	58.0827	0.37296
Chi-Chi, Taiwan	1999	7.62	TCU060-X.AT2	25.3669	52.5121	0.15295	38.0389	0.2536
Chi-Chi, Taiwan	1999	7.62	TCU061-X.AT2	29.5766	60.1331	0.1368	40.4159	0.30127
Chi-Chi, Taiwan	1999	7.62	TCU064-X.AT2	33.8589	63.7621	0.11836	47.6283	0.41034
Chi-Chi, Taiwan	1999	7.62	TCU065-X.AT2	24.0605	53.8185	0.66597	101.0385	0.15471
Chi-Chi, Taiwan	1999	7.62	TCU067-X.AT2	23.625	42.496	0.41222	72.4706	0.17927
Chi-Chi, Taiwan	1999	7.62	TCU068-X.AT2	32.1895	53.0202	0.52567	204.4998	0.39669
Chi-Chi, Taiwan	1999	7.62	TCU071-X.AT2	23.1169	54.8347	0.61177	56.5315	0.094228
Chi-Chi, Taiwan	1999	7.62	TCU072-X.AT2	8.7339	20.1532	0.081469	8.087	0.10122
Chi-Chi, Taiwan-02	1999	5.90	TCU074-X.AT2	34.6573	49.6089	0.44299	54.1246	0.12459
Chi-Chi, Taiwan	1999	7.62	TCU075-X.AT2	25.2218	44.4556	0.293	58.4349	0.20337
Chi-Chi, Taiwan	1999	7.62	TCU076-X.AT2	24.9315	43.875	0.35916	58.711	0.16669
Chi-Chi, Taiwan-03	1999	6.20	TCU078-X.AT2	2.3427	12.4476	0.41278	25.5283	0.063064
Chi-Chi, Taiwan-03	1999	6.20	TCU079-X.AT2	3	14.9355	0.29177	14.4922	0.050649
Chi-Chi, Taiwan-06	1999	6.30	TCU080-X.AT2	6.0887	18.9919	0.54755	29.1859	0.054354
Chi-Chi, Taiwan	1999	7.62	TCU081-X.AT2	35.0202	60.7863	0.086297	35.8468	0.42358
Chi-Chi, Taiwan	1999	7.62	TCU082-X.AT2	25.3669	46.2702	0.21446	52.4924	0.2496
Chi-Chi, Taiwan-03	1999	6.20	TCU084-X.AT2	5.7661	22.4597	0.10601	17.5519	0.16883
Chi-Chi, Taiwan	1999	7.62	TCU087-X.AT2	30.8831	54.1815	0.11685	44.5181	0.38849
Chi-Chi, Taiwan	1999	7.62	TCU088-X.AT2	30.6774	55.7742	0.50604	19.6122	0.03952
Chi-Chi, Taiwan-03	1999	6.20	TCU089-X.AT2	5.6048	26.0081	0.0865	7.0141	0.082687
Chi-Chi, Taiwan	1999	7.62	TCU094-X.AT2	38.504	57.8831	0.082525	31.3058	0.38683
Chi-Chi, Taiwan	1999	7.62	TCU096-X.AT2	34.0766	58.3911	0.081524	31.5054	0.39408
Chi-Chi, Taiwan	1999	7.62	TCU098-X.AT2	38.8669	63.7621	0.10738	35.8347	0.34028

Earthquake Name	Year	Mag	File Name	Start time (s)	End Time (s)	GMRotIPGA (g)	GMRotIPGV (cm/s)	GMRotIPGV/GMRotIPGA (s)
Chi-Chi, Taiwan	1999	7.62	TCU100-X.AT2	25.5847	59.7702	0.1181	38.1826	0.32968
Chi-Chi, Taiwan	1999	7.62	TCU101-X.AT2	14.4556	30.9073	0.22402	57.1311	0.26006
Chi-Chi, Taiwan	1999	7.62	TCU102-X.AT2	33.1331	52.3669	0.24591	87.6956	0.36364
Chi-Chi, Taiwan	1999	7.62	TCU103-X.AT2	31.9718	56.5766	0.15636	44.092	0.28755
Chi-Chi, Taiwan	1999	7.62	TCU104-X.AT2	27.254	61.5121	0.10594	43.6065	0.41974
Chi-Chi, Taiwan	1999	7.62	TCU105-X.AT2	29.9395	61.2944	0.12194	38.6022	0.32282
Chi-Chi, Taiwan	1999	7.62	TCU109-X.AT2	41.4073	62.6734	0.16827	51.5689	0.3125
Chi-Chi, Taiwan	1999	7.62	TCU110-X.AT2	29.7218	55.4879	0.18221	57.9197	0.32415
Chi-Chi, Taiwan	1999	7.62	TCU120-X.AT2	25.2218	47.7218	0.22957	47.8138	0.21238
Chi-Chi, Taiwan	1999	7.62	TCU122-X.AT2	24.5685	46.7782	0.23128	38.7456	0.17083
Chi-Chi, Taiwan	1999	7.62	TCU128-X.AT2	31.8266	58.0282	0.15406	66.0945	0.43749
Chi-Chi, Taiwan	1999	7.62	TCU129-X.AT2	24.2782	43.5121	0.80029	47.0219	0.059915
Chi-Chi, Taiwan	1999	7.62	TCU136-X.AT2	31.6815	60.7863	0.16915	48.4059	0.29181
Chi-Chi, Taiwan	1999	7.62	TCU138-X.AT2	26.1895	60.6653	0.20758	39.2026	0.19258
Chi-Chi, Taiwan	1999	7.62	WNT-X.AT2	9.121	19.8145	0.75877	52.444	0.07048
Northridge-01	1994	6.69	WPI-X.AT2	3.377	11.2198	0.38477	78.1146	0.20702
N. Palm Springs	1986	6.06	WWT-X.AT2	1.2399	6.0181	0.60831	33.0306	0.055369

### 3.5 VALIDATION EXERCISE

Purvance et al. [2008] simulated the rocking and overturning responses of 2D rectangular blocks exposed to horizontal forcing. That work parameterized the fragilities as functions of block geometrical parameters, PGA, and PGV/PGA. In addition, Purvance et al. [2008] validated those results through shake-table experiments. In order to ensure that *Rigid* accurately calculates rocking and overturning responses and that the fragilities as determined by this waveform set are representative of those presented in Purvance et al. [2008], rectangular blocks were simulated. In particular, 1 m tall, rectangular blocks with height-to-width ratios of 9.96, 4.93, 3.23, and 2.37 were constructed in Google SketchUp. These blocks have corresponding alphas of 0.1 rad, 0.2 rad, 0.3 rad, and 0.4 rad, respectively, where alpha is the angle from the line connecting the center of mass to the rocking point and vertical (see Purvance et al. [2008] for additional information). Figure 3.11 shows the rectangular block models imported into *Rigid*. The damping coefficient was set to 2.0 and coefficient of friction set to 0.6 in these simulations. In addition,  $K_N = K_S = 10^{-8}$  N/m, and the density is  $2600 \text{ kg/m}^3$ . These material property values are the same as those used in the subsequent fragility modeling for Yucca Mountain features. Scaling is taken from 0.1g, in 0.1g increments, to 2g or until 10 consecutive failures (e.g., overturning probability = 1) was obtained. Only the  $x$  components of the recordings were used to mimic the results of Purvance et al. [2008], and  $\text{GMRotI}_{\text{PGA}}$  and  $\text{GMRotI}_{\text{PGV}}$  were replaced by the PGA and PGV of that recording.

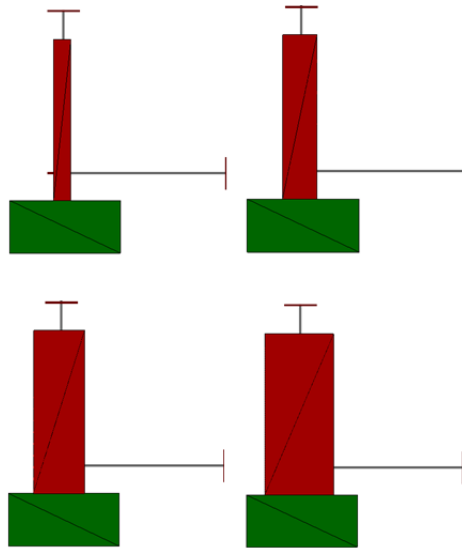


Figure 3.11 The rectangular block models for validation exercise imported into *Rigid*.

Figure 3.12 demonstrates the fragilities obtained from this set of waveforms. Nine bins were taken in PGV/PGA, and the average overturning probabilities for each PGA were obtained within each bin. In this figure, as was done previously,  $\text{GMRotI}_{\text{PGA}}$  and  $\text{GMRotI}_{\text{PGV}}$  were replaced by the PGA and PGV. The boxes are colored relative to the overturning probability. The red and green lines correspond to the 1% and 99% overturning probability contours of Purvance et al. [2008], respectively. The dashed red and green lines are the 95% confidence intervals on the parameterizations of Purvance et al. [2008] for the 1% (lower 95% confidence

interval) and 99% (higher 95% confidence interval). The visual agreement is quite good considering that the restitution models implemented in *Rigid* and Purvance et al. [2008] are significantly different. In addition, sliding and free flight can occur in *Rigid* whereas those modes of motion are not allowed in the Purvance et al. [2008] simulations.

Figure 3.13 demonstrates the difference of the median Purvance et al. [2008] derived overturning probabilities and those obtained via *Rigid*. Thus a difference greater than 0 (hotter than green) means that the Purvance et al. [2008] model produced a more fragile estimate, while values less than 0 (cooler than green) show that the *Rigid*-based fragilities were more fragile. For alpha 0.1 rad and 0.2 rad, the Purvance et al. [2008] model produced generally higher overturning probabilities. There are some instances for the cases of alpha 0.3 rad and 0.4 rad, however, where the *Rigid* models produced somewhat higher overturning probabilities (blue symbols). These cases occurred in the transition region from no overturning to overturning, but note that these differences are small. Over the whole data set as represented in Figure 3.13, the average probability mismatches are  $0.03 \pm 0.12$ ,  $0.02 \pm 0.08$ ,  $0.02 \pm 0.10$ , and  $0.03 \pm 0.14$  for alpha 0.1 rad, 0.2 rad, 0.3 rad, and 0.4 rad, respectively. Likely the various coefficient-of-restitution models caused these slight differences. Regardless, these tests demonstrate that the fragilities of Purvance et al. [2008] and those determined by *Rigid* are very similar. Thus it is concluded that *Rigid* has been validated, as the Purvance et al. [2008] fragilities have been validated via shake-table experiments. Future validation exercises would expand upon the Purvance et al. [2008] experiments to include multi-block stacks and 3D ground motion time histories.

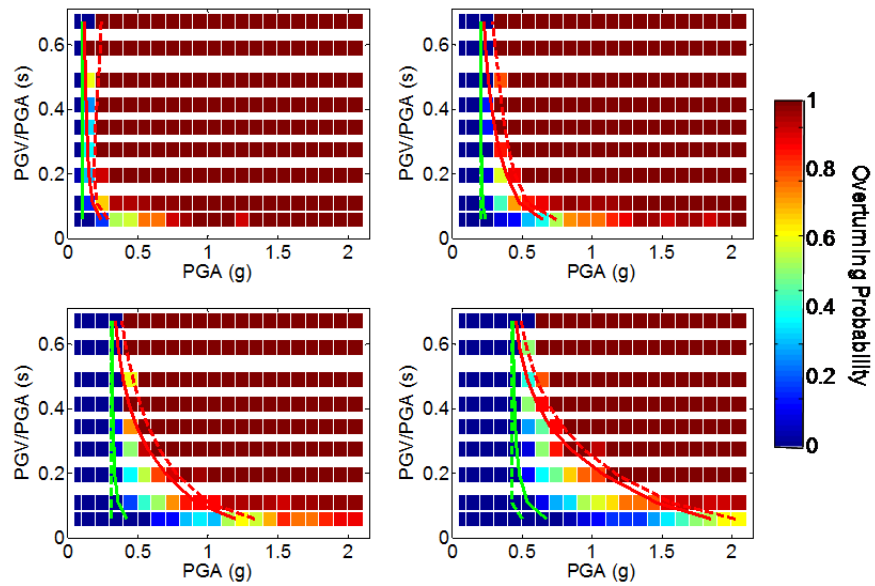


Figure 3.12 Fragilities for the rectangular blocks shown in Figure 3.2 obtained from the waveforms used in shake-table experiments.

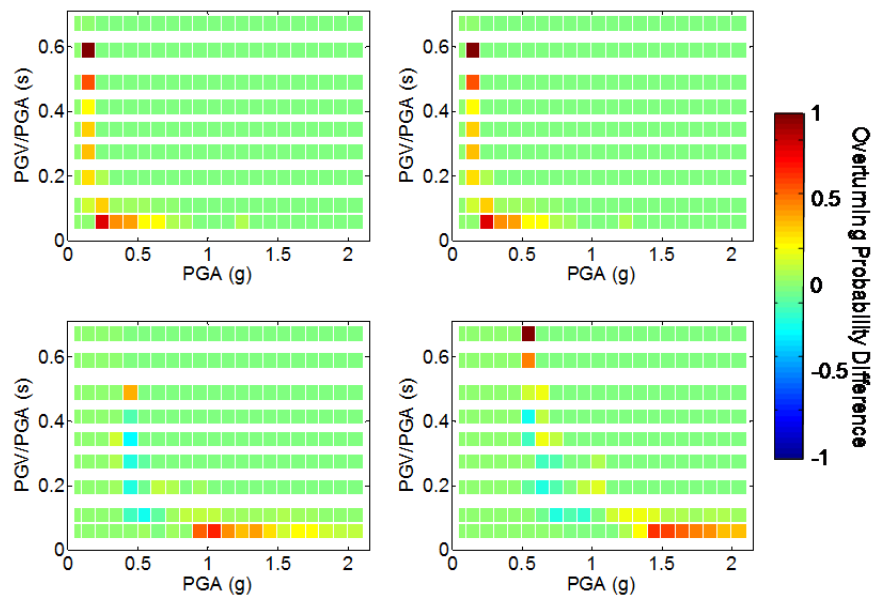


Figure 3.13 The difference of the median Purvance et al. [2008] derived overturning probabilities and those obtained via *Rigid*.

### 3.6 FRAGILITY RESULTS

As outline above, photogrammetry was used to delineate the geometries of fragile geological features on Yucca Mountain and object models were developed. These objects include: Fluffy, Len stack, Matt Cubed, Nichole, Pillow, S\_Yucca\_2, Sue, Tripod, and Whitney. Figures 3.2 through 3.10 show these fragile geological figures along with the object models used in the fragility computations. Prior to batch fragility calculations, the object models were equilibrated without forcing applied to the fixed blocks. In addition, the equilibrate checkbox was checked in the user interface wherein extra damping is applied based on the local damping model used in 3DEC [Itasca Consulting Group 2008]. After equilibrium was reached, the model configurations were saved as .msf files. Thus the object model representations shown in Figures 3.2 through 3.10 are the models in their equilibrated states. Prior to the simulation of each ground motion time history at each scaling factor, the object model has been reset to this equilibrium configuration. The overturning fragilities for each of these objects are presented in Figure 3.14. Note that these correspond to nine equally spaced bins in  $GMRotI_{PGV}/GMRotI_{PGA}$  and the averages of the  $GMRotI_{PGV}/GMRotI_{PGA}$  values of the data in those bins are presented.

As demonstrated in Figure 3.15, the most fragile objects analyzed in this analysis are Matt Cubed, Tripod, and Whitney. It is very interesting to note that Fluffy, Len stack, S\_Yucca\_2, and Sue demonstrate very similar fragilities even though their failure mechanisms may be very different. For instance, Sue fails primarily from sliding whereas Fluffy and S\_Yucca\_2 fail due to rocking motion. Len stack, on the other hand, fails in a complex fashion due to frictional contact between the object components and the back wall. These less fragile objects have similar fragilities to the symmetric, 1 m tall, rectangular blocks with height-to-width ratios of 2.37 (0.4 rad alpha values) shown in Figure 3.12.

Quantitatively assessing the uncertainty in these fragility estimates is rather difficult without physical experiments. The previous effort of Purvance et al. [2008] calculated the uncertainty associated with the fragility parameterization. When comparing PBRs with seismic hazard estimates, Purvance et al. [2008] included the uncertainties associated with center-of-mass locations based on the findings of Purvance [2005]; that work demonstrated that alpha may be uncertain by 10–20% due to estimation of the center-of-mass locations by eye. In this work, though, such parameterization uncertainties and center-of-mass location uncertainties are not present. Instead, the uncertainties lie in the geometric representation of the objects and the physical assumptions of *Rigid*. It is clear that the modeled contact configurations are not the actual contact configurations. In addition, the coefficient of friction and damping factor are uncertain. The normal and shear stiffness values have been set so that the time step is not too small, while at the same time, it is adequately small so that contacts will be detected with minimal overlap.

Although *Rigid* is efficient, it has not been feasible to undertake parametric searches to determine the effects of these uncertainties on the fragility estimates. For instance, one could create a number of different representations of the object models and simulate the responses with a suite of physical assumptions. To date this effort has not been undertaken. An alternate and perhaps more fruitful method to assess uncertainty would be through physical experiments. For instance, a number of objects could be tested with 3D ground motions on the shake table and compared with an object model. Such an effort is beyond the scope of the work presented herein.

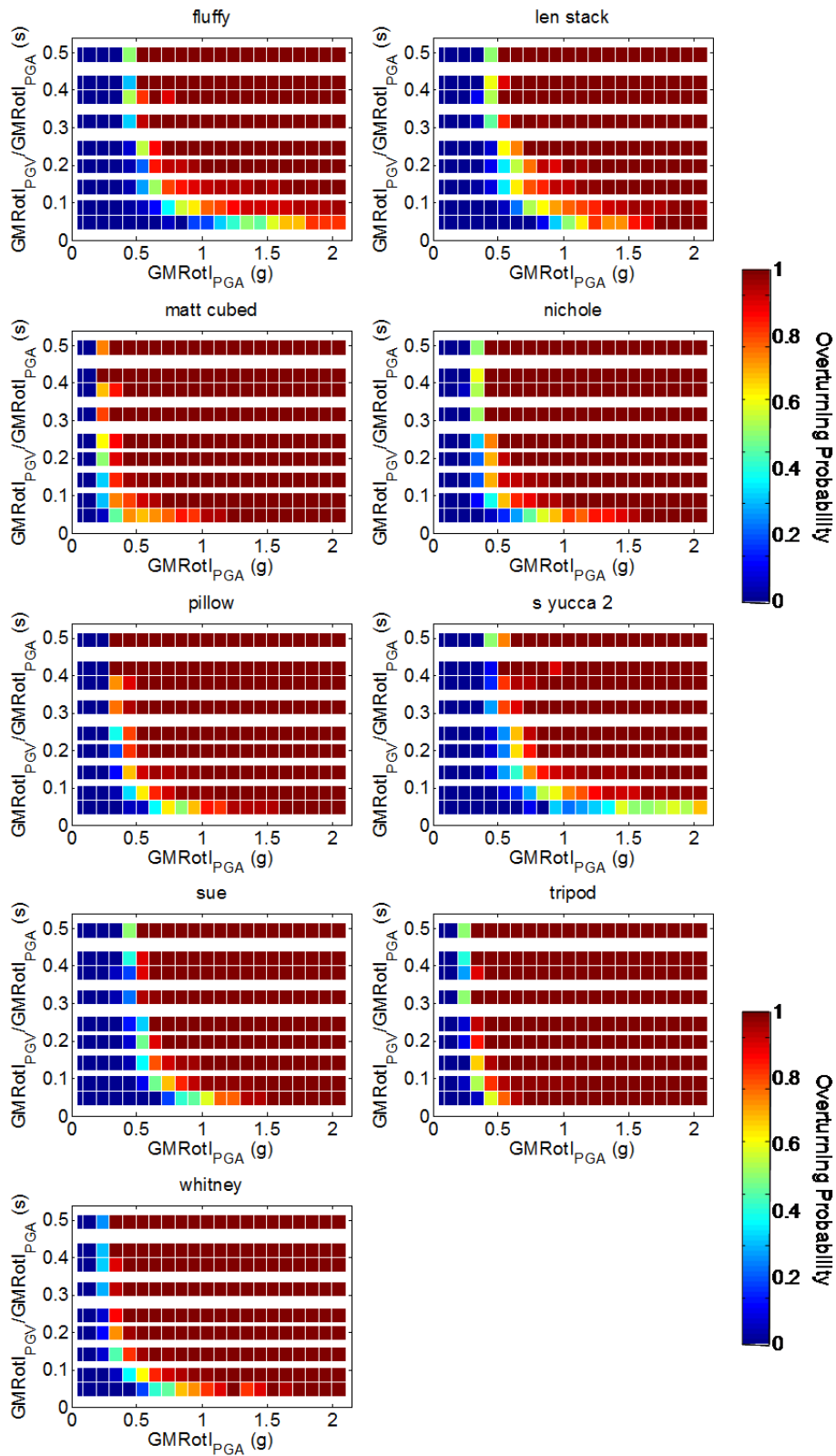


**Figure 3.14** Overturning fragilities for class 2 rocks Fluffy, Matt Cubed, Nichole, Pillow, Sue, and S\_Yucca2, and Class 3 rock stacks Len, Tripod, and Whitney.

## REFERENCES

- Andrews, DJ, TC Hanks, and JW Whitney (2007). Physical limits on ground motion at Yucca Mountain. *Bull. Seism. Soc. Am.* 97(6):1771–1792.
- Anooshehpour, A, MD Purvance, JN Brune, LA Preston, JG Anderson, and KD Smith (2006). Precarious rock methodology for seismic hazard: physical testing, numerical modeling and coherence studies, DOE/NSHE Cooperative Agreement Task ORD-FY04–020, *Final Technical Report TR–06–003*.
- Anooshehpour, A, JN Brune, and Y Zeng (2004). Methodology for obtaining constraints on ground motion from precariously balanced rocks, *Bull. Seism. Soc. Am.*, 94(1):285–303.
- Anooshehpour, A, JN Brune, and DH Von Seggern (2002). Constraints on ground motion at Yucca Mountain provided by precarious rocks, DOE/NSHE Cooperative Agreement Number DE-FC08-98NV12081, *Report TR–02–001*.
- Anooshehpour, A, MD Purvance, JN Brune, and T Rennie (2007). Reduction in the uncertainties in the ground motion constraints by improved field-testing techniques of precariously balanced rocks, *Proc.*, 2007 SCEC Annual Meeting, September 9-12. Palm Springs.
- Bell, JW, JN Brune, T Liu, M Zerda, and JC Yount (1998). Dating the precariously balanced rocks in seismically active parts of California and Nevada, *Geology*, 26:495–498.
- Blow, J, and AJ Binstock (2004). How to find the inertia tensor (or other mass properties) of a 3D solid body represented by a triangle mesh, <http://www.number-none.com/blow/inertia/index.html> last visited on 12/4/2009.
- Boore, DM, J Watson-Lamprey, and NA Abrahamson (2006). Orientation-independent measures of ground motion, *Bull. Seism. Soc. Am.* 96(4A):1502–1511.
- Brune, JN (1996). Precariously balanced rocks and ground motion maps for southern California, *Bull. Seism. Soc. Am.*, 86(1):43–54.
- Brune, JN, and JW Whitney (2000). Precarious Rocks and seismic shaking at Yucca Mountain, Nevada, *USGS Digital Data Series*, Vol. 058, Chapter M.
- Buss, SR (2000). Accurate and efficient simulation of rigid-body rotations, *J. Computational Phys.*, 164:377–406.
- Cundall, PA (1971). A computer model for simulating progressive large-scale movements in block rock mechanics, *Proceedings of the Symposium of International Society of Rock Mechanics*, Vol. 8, Nancy, France.
- Cundall, PA (1988). Formulation of a three-dimensional distinct element model. Part I: a scheme to detect and represent contacts in a system composed of many polyhedral blocks, *Inter. J. Rock Mech., and Mining Sciences and Geomechanics Abstracts*, 25(3):107–116.
- Cundall, PA, ODL Strack (1979). A discrete numerical model for granular assemblies, *Geotechnique*, 29(1):47–65.
- Gilardi, G, and I. Sharf (2002). Literature survey of contact dynamics modeling, *Mechanism and Machine Theory*, 37:1213–1239.
- Guzzetti, F, G Crosta, R Detti, and F Agliardi (2002). STONE: a computer program for the three-dimensional simulation of rock-falls, *Computers and Geosciences*, 28:1079–1093.
- Hanks, T, and N. Abrahamson (2010). *Review of ExGM Research Program and Summary of Final Report*, September 11, 2010: 2010 SCEC Annual Meeting: Extreme Ground Motion (ExGM) Workshop: The Last Hurrah, 2010 SCEC ExGM Meeting, Palm Springs.
- Itasca Consulting Group, Inc. (2009). UDEC (Universal Distinct Element Code), Version 4.1. Minneapolis: ICG.
- Itasca Consulting Group, Inc. (2008). 3DEC (Three Dimensional Distinct Element Code), Version 4.2. Minneapolis: ICG.

- Johnson, SM, JR Williams, and BK Cook (2008). Quaternion-based rigid body rotation integration algorithms for use in particle methods, *Inter. J. Numerical Methods in Engrg.*, 74:1303–1313.
- Lankarani, HM, and PE Nikraves (1990). A contact force model with hysteresis damping for impact analysis of multibody systems, *J. Mechanical Design*, 112:369–376.
- Munjiza, A, JP Latham, and NWM John (2003). 3D dynamics of discrete element systems comprising irregular discrete elements-integration solution for finite rotations in 3D, *Inter. J. Numerical Methods in Engrg.*, 56:35–55.
- Nezami, EG, YMA Hashash, D Zhao, and J. Ghaboussi (2004). A fast contact detection algorithm for 3-D discrete element method, *Computers and Geotechnics*, 31:575–587.
- Nezami, EG, YMA Hashash, and D. Zhao (2006). Shortest link method for contact detection in discrete element method. *Inter. J. Numerical Methods in Geomechanics*, 30:783–801.
- Psycharis, IN, JV Lemos, DY Papastamatiou, C Zambas, and C. Papantonopoulos (2003). Numerical study of the seismic behaviour of a part of the Parthenon Pronaos, *Earthq. Engrg. Struct. Dyn.*, 32:2063–2084.
- Purvance, MD, R Anooshehpour, and JN Brune (2006). Precariously balanced rock methodology and shake table calibration, *Seism. Res. Letts.*, 77 (2), p. 247.
- Purvance, MD (2005). *Overturing of Slender Blocks: Numerical Investigation and Application to Precariously Balanced Rocks in Southern California*, Ph.D. Dissertation, University of Nevada, Reno, Reno, Nevada (<http://www.seismo.unr.edu/gradresearch.html>).
- Purvance, MD, and JN Brune (2007) Fragility estimation for precipitous cliffs and a rock stack on Yucca Mountain, Nevada, in Proceedings 2007 SCEC Annual Meeting, September 9-12. Palm Springs.
- Rood, DH, RC Finkel, and G Balco (2009) Evaluation of past seismic activity at Yucca Mountain, Nevada, based on the rate of landscape evolution determined with cosmogenic Cl-36 and Ne-21 in feldspar mineral separates, *Seismological Research Letters*, 80, 2, 379.
- Stepp, JC, I Wong, J Whitney, R Quittmeyer, N Abrahamson, G Toro, R Youngs, K Coppersmith, J Savy, T Sullivan, and Yucca Mountain PSHA Project Members (2001). Probabilistic seismic hazard analyses for fault displacement and ground motions at Yucca Mountain, Nevada, *Earthq. Spectra*, 17:113–152.
- Wong, I (2004). Development of earthquake ground motion input for preclosure seismic design and postclosure performance assessment of a geological repository at Yucca Mountain, Nevada. Report to the DOE, Report # MDL-MGR-GS-000003, REV 01, DOI 10.2172/837491 available at [http://www.osti.gov/energycitations/product.biblio.jsp?osti\\_id=837491](http://www.osti.gov/energycitations/product.biblio.jsp?osti_id=837491).

## APPENDIX

Relatively accurate shapes of the fragile geologic features are determined using *PhotoModeler* photogrammetry software. This image-based modeling software creates 3D shapes of rocks from the digital pictures of the rocks taken from different angles. The following steps outline the procedure:

1. Place paper targets with unique images on the rock. The laminated targets are attached to the rock surface using strapping tape. For most rock, a more efficient way is to wrap a fabric with patterns around the rock. The patterns that do not repeat too frequently and have geometric shapes with sharp corners are preferred. This would allow easy selection of common points between photographs during shape calculation. Figure 2.2 shows the usage of targets and the fabric on the rocks.
2. Introduce a coordinate system and a scale near the rocks. The coordinate system consists of three orthogonal 1/4-in. aluminum rods mounted on a tripod. Distances of 1 ft (~30 cm) marked on each rod are used as the modeling scale. For consistency, we have used the *convention* of pointing the *X*-axis in the North direction and the *Z*-axis in the vertical direction. (In earlier studies we used a plumb bulb to represent the vertical *only*.) When taking pictures, make sure that the coordinates are visible in at least three photographs.
3. Use a pre-calibrated digital camera to take pictures of the rock at approximately 15° intervals and a distance of about 3 m. Make sure that the camera settings are exactly the same as those used during the calibration.
4. Follow *PhotoModeler* instructions to generate 3D models of the stand-alone rocks and their pedestals, as well as the individual rocks in a stack. The *PhotoModeler* software uses the selected points on the rock surface to generate convex or flat surfaces that are composed of triangles. The concave surfaces are modeled as flat or convex surfaces using the highest points on that surface. Therefore, to avoid overestimating the volume of the rocks, extreme care must be taken when the rocks have concave surfaces. There are simple ways to make first order corrections to concave shapes. Fortunately, the majority of rocks in the project have round or rectangular shapes and corrections are not necessary.



## PEER REPORTS

PEER reports are available individually or by yearly subscription. PEER reports can be ordered at [http://peer.berkeley.edu/publications/peer\\_reports.html](http://peer.berkeley.edu/publications/peer_reports.html) or by contacting the Pacific Earthquake Engineering Research Center, 325 Davis Hall mail code 1792, Berkeley, CA 94720. Tel.: (510) 642-3437; Fax: (510) 665-1655; Email: peer\_editor@berkeley.edu

- PEER 2012/06** *Fragilities for Precarious Rocks at Yucca Mountain.* Matthew D. Purvance, Rasool Anooshehpour, and James N. Brune. December 2012.
- PEER 2012/05** *Development of Simplified Analysis Procedure for Piles in Laterally Spreading Layered Soils.* Christopher R. McGann, Pedro Arduino, and Peter Mackenzie-Helnwein. December 2012.
- PEER 2012/04** *Unbonded Pre-Tensioned Columns for Bridges in Seismic Regions.* Phillip M. Davis, Todd M. Janes, Marc O. Eberhard, and John F. Stanton. December 2012.
- PEER 2012/03** *Experimental and Analytical Studies on Reinforced Concrete Buildings with Seismically Vulnerable Beam-Column Joints.* Sangjoon Park and Khalid M. Mosalam. October 2012.
- PEER 2012/02** *Seismic Performance of Reinforced Concrete Bridges Allowed to Uplift during Multi-Directional Excitation.* Andres Oscar Espinoza and Stephen A. Mahin. July 2012.
- PEER 2012/01** *Spectral Damping Scaling Factors for Shallow Crustal Earthquakes in Active Tectonic Regions.* Sanaz Rezaeian, Yousef Bozorgnia, I. M. Idriss, Kenneth Campbell, Norman Abrahamson, and Walter Silva. July 2012.
- PEER 2011/10** *Earthquake Engineering for Resilient Communities: 2011 PEER Internship Program Research Report Collection.* Eds. Heidi Faison and Stephen A. Mahin. December 2011.
- PEER 2011/09** *Calibration of Semi-Stochastic Procedure for Simulating High-Frequency Ground Motions.* Jonathan P. Stewart, Emel Seyhan, and Robert W. Graves. December 2011.
- PEER 2011/08** *Water Supply in regard to Fire Following Earthquake.* Charles Scawthorn. November 2011.
- PEER 2011/07** *Seismic Risk Management in Urban Areas. Proceedings of a U.S.-Iran-Turkey Seismic Workshop.* September 2011.
- PEER 2011/06** *The Use of Base Isolation Systems to Achieve Complex Seismic Performance Objectives.* Troy A. Morgan and Stephen A. Mahin. July 2011.
- PEER 2011/05** *Case Studies of the Seismic Performance of Tall Buildings Designed by Alternative Means.* Task 12 Report for the Tall Buildings Initiative. Jack Moehle, Yousef Bozorgnia, Nirmal Jayaram, Pierson Jones, Mohsen Rahnama, Nilesh Shome, Zeynep Tuna, John Wallace, Tony Yang, and Farzin Zareian. July 2011.
- PEER 2011/04** *Recommended Design Practice for Pile Foundations in Laterally Spreading Ground.* Scott A. Ashford, Ross W. Boulanger, and Scott J. Brandenburg. June 2011.
- PEER 2011/03** *New Ground Motion Selection Procedures and Selected Motions for the PEER Transportation Research Program.* Jack W. Baker, Ting Lin, Shrey K. Shahi, and Nirmal Jayaram. March 2011.
- PEER 2011/02** *A Bayesian Network Methodology for Infrastructure Seismic Risk Assessment and Decision Support.* Michelle T. Bensi, Armen Der Kiureghian, and Daniel Straub. March 2011.
- PEER 2011/01** *Demand Fragility Surfaces for Bridges in Liquefied and Laterally Spreading Ground.* Scott J. Brandenburg, Jian Zhang, Pirooz Kashighandi, Yili Huo, and Minxing Zhao. March 2011.
- PEER 2010/05** *Guidelines for Performance-Based Seismic Design of Tall Buildings.* Developed by the Tall Buildings Initiative. November 2010.
- PEER 2010/04** *Application Guide for the Design of Flexible and Rigid Bus Connections between Substation Equipment Subjected to Earthquakes.* Jean-Bernard Dastous and Armen Der Kiureghian. September 2010.
- PEER 2010/03** *Shear Wave Velocity as a Statistical Function of Standard Penetration Test Resistance and Vertical Effective Stress at Caltrans Bridge Sites.* Scott J. Brandenburg, Naresh Bellana, and Thomas Shantz. June 2010.
- PEER 2010/02** *Stochastic Modeling and Simulation of Ground Motions for Performance-Based Earthquake Engineering.* Sanaz Rezaeian and Armen Der Kiureghian. June 2010.
- PEER 2010/01** *Structural Response and Cost Characterization of Bridge Construction Using Seismic Performance Enhancement Strategies.* Ady Aviram, Božidar Stojadinović, Gustavo J. Parra-Montesinos, and Kevin R. Mackie. March 2010.
- PEER 2009/03** *The Integration of Experimental and Simulation Data in the Study of Reinforced Concrete Bridge Systems Including Soil-Foundation-Structure Interaction.* Matthew Dryden and Gregory L. Fenves. November 2009.

- PEER 2009/02** *Improving Earthquake Mitigation through Innovations and Applications in Seismic Science, Engineering, Communication, and Response. Proceedings of a U.S.-Iran Seismic Workshop.* October 2009.
- PEER 2009/01** *Evaluation of Ground Motion Selection and Modification Methods: Predicting Median Interstory Drift Response of Buildings.* Curt B. Haselton, Ed. June 2009.
- PEER 2008/10** *Technical Manual for Strata.* Albert R. Kottke and Ellen M. Rathje. February 2009.
- PEER 2008/09** *NGA Model for Average Horizontal Component of Peak Ground Motion and Response Spectra.* Brian S.-J. Chiou and Robert R. Youngs. November 2008.
- PEER 2008/08** *Toward Earthquake-Resistant Design of Concentrically Braced Steel Structures.* Patxi Uriz and Stephen A. Mahin. November 2008.
- PEER 2008/07** *Using OpenSees for Performance-Based Evaluation of Bridges on Liquefiable Soils.* Stephen L. Kramer, Pedro Arduino, and HyungSuk Shin. November 2008.
- PEER 2008/06** *Shaking Table Tests and Numerical Investigation of Self-Centering Reinforced Concrete Bridge Columns.* Hyung IL Jeong, Junichi Sakai, and Stephen A. Mahin. September 2008.
- PEER 2008/05** *Performance-Based Earthquake Engineering Design Evaluation Procedure for Bridge Foundations Undergoing Liquefaction-Induced Lateral Ground Displacement.* Christian A. Ledezma and Jonathan D. Bray. August 2008.
- PEER 2008/04** *Benchmarking of Nonlinear Geotechnical Ground Response Analysis Procedures.* Jonathan P. Stewart, Annie On-Lei Kwok, Youssef M. A. Hashash, Neven Matasovic, Robert Pyke, Zhiliang Wang, and Zhaohui Yang. August 2008.
- PEER 2008/03** *Guidelines for Nonlinear Analysis of Bridge Structures in California.* Ady Aviram, Kevin R. Mackie, and Božidar Stojadinović. August 2008.
- PEER 2008/02** *Treatment of Uncertainties in Seismic-Risk Analysis of Transportation Systems.* Evangelos Stergiou and Anne S. Kiremidjian. July 2008.
- PEER 2008/01** *Seismic Performance Objectives for Tall Buildings.* William T. Holmes, Charles Kircher, William Petak, and Nabih Youssef. August 2008.
- PEER 2007/12** *An Assessment to Benchmark the Seismic Performance of a Code-Conforming Reinforced Concrete Moment-Frame Building.* Curt Haselton, Christine A. Goulet, Judith Mitrani-Reiser, James L. Beck, Gregory G. Deierlein, Keith A. Porter, Jonathan P. Stewart, and Ertugrul Taciroglu. August 2008.
- PEER 2007/11** *Bar Buckling in Reinforced Concrete Bridge Columns.* Wayne A. Brown, Dawn E. Lehman, and John F. Stanton. February 2008.
- PEER 2007/10** *Computational Modeling of Progressive Collapse in Reinforced Concrete Frame Structures.* Mohamed M. Talaat and Khalid M. Mosalam. May 2008.
- PEER 2007/09** *Integrated Probabilistic Performance-Based Evaluation of Benchmark Reinforced Concrete Bridges.* Kevin R. Mackie, John-Michael Wong, and Božidar Stojadinović. January 2008.
- PEER 2007/08** *Assessing Seismic Collapse Safety of Modern Reinforced Concrete Moment-Frame Buildings.* Curt B. Haselton and Gregory G. Deierlein. February 2008.
- PEER 2007/07** *Performance Modeling Strategies for Modern Reinforced Concrete Bridge Columns.* Michael P. Berry and Marc O. Eberhard. April 2008.
- PEER 2007/06** *Development of Improved Procedures for Seismic Design of Buried and Partially Buried Structures.* Linda Al Atik and Nicholas Sitar. June 2007.
- PEER 2007/05** *Uncertainty and Correlation in Seismic Risk Assessment of Transportation Systems.* Renee G. Lee and Anne S. Kiremidjian. July 2007.
- PEER 2007/04** *Numerical Models for Analysis and Performance-Based Design of Shallow Foundations Subjected to Seismic Loading.* Sivapalan Gajan, Tara C. Hutchinson, Bruce L. Kutter, Prishati Raychowdhury, José A. Ugalde, and Jonathan P. Stewart. May 2008.
- PEER 2007/03** *Beam-Column Element Model Calibrated for Predicting Flexural Response Leading to Global Collapse of RC Frame Buildings.* Curt B. Haselton, Abbie B. Liel, Sarah Taylor Lange, and Gregory G. Deierlein. May 2008.
- PEER 2007/02** *Campbell-Bozorgnia NGA Ground Motion Relations for the Geometric Mean Horizontal Component of Peak and Spectral Ground Motion Parameters.* Kenneth W. Campbell and Yousef Bozorgnia. May 2007.
- PEER 2007/01** *Boore-Atkinson NGA Ground Motion Relations for the Geometric Mean Horizontal Component of Peak and Spectral Ground Motion Parameters.* David M. Boore and Gail M. Atkinson. May 2007.
- PEER 2006/12** *Societal Implications of Performance-Based Earthquake Engineering.* Peter J. May. May 2007.

- PEER 2006/11** *Probabilistic Seismic Demand Analysis Using Advanced Ground Motion Intensity Measures, Attenuation Relationships, and Near-Fault Effects.* Polsak Tothong and C. Allin Cornell. March 2007.
- PEER 2006/10** *Application of the PEER PBEE Methodology to the I-880 Viaduct.* Sashi Kunnath. February 2007.
- PEER 2006/09** *Quantifying Economic Losses from Travel Forgone Following a Large Metropolitan Earthquake.* James Moore, Sungbin Cho, Yue Yue Fan, and Stuart Werner. November 2006.
- PEER 2006/08** *Vector-Valued Ground Motion Intensity Measures for Probabilistic Seismic Demand Analysis.* Jack W. Baker and C. Allin Cornell. October 2006.
- PEER 2006/07** *Analytical Modeling of Reinforced Concrete Walls for Predicting Flexural and Coupled-Shear-Flexural Responses.* Kutay Orakcal, Leonardo M. Massone, and John W. Wallace. October 2006.
- PEER 2006/06** *Nonlinear Analysis of a Soil-Drilled Pier System under Static and Dynamic Axial Loading.* Gang Wang and Nicholas Sitar. November 2006.
- PEER 2006/05** *Advanced Seismic Assessment Guidelines.* Paolo Bazzurro, C. Allin Cornell, Charles Menun, Maziar Motahari, and Nicolas Luco. September 2006.
- PEER 2006/04** *Probabilistic Seismic Evaluation of Reinforced Concrete Structural Components and Systems.* Tae Hyung Lee and Khalid M. Mosalam. August 2006.
- PEER 2006/03** *Performance of Lifelines Subjected to Lateral Spreading.* Scott A. Ashford and Teerawut Juirnarongrit. July 2006.
- PEER 2006/02** *Pacific Earthquake Engineering Research Center Highway Demonstration Project.* Anne Kiremidjian, James Moore, Yue Yue Fan, Nesrin Basoz, Ozgur Yazali, and Meredith Williams. April 2006.
- PEER 2006/01** *Bracing Berkeley. A Guide to Seismic Safety on the UC Berkeley Campus.* Mary C. Comerio, Stephen Tobriner, and Ariane Fehrenkamp. January 2006.
- PEER 2005/16** *Seismic Response and Reliability of Electrical Substation Equipment and Systems.* Junho Song, Armen Der Kiureghian, and Jerome L. Sackman. April 2006.
- PEER 2005/15** *CPT-Based Probabilistic Assessment of Seismic Soil Liquefaction Initiation.* R. E. S. Moss, R. B. Seed, R. E. Kayen, J. P. Stewart, and A. Der Kiureghian. April 2006.
- PEER 2005/14** *Workshop on Modeling of Nonlinear Cyclic Load-Deformation Behavior of Shallow Foundations.* Bruce L. Kutter, Geoffrey Martin, Tara Hutchinson, Chad Harden, Sivapalan Gajan, and Justin Phalen. March 2006.
- PEER 2005/13** *Stochastic Characterization and Decision Bases under Time-Dependent Aftershock Risk in Performance-Based Earthquake Engineering.* Gee Liek Yeo and C. Allin Cornell. July 2005.
- PEER 2005/12** *PEER Testbed Study on a Laboratory Building: Exercising Seismic Performance Assessment.* Mary C. Comerio, editor. November 2005.
- PEER 2005/11** *Van Nuys Hotel Building Testbed Report: Exercising Seismic Performance Assessment.* Helmut Krawinkler, editor. October 2005.
- PEER 2005/10** *First NEES/E-Defense Workshop on Collapse Simulation of Reinforced Concrete Building Structures.* September 2005.
- PEER 2005/09** *Test Applications of Advanced Seismic Assessment Guidelines.* Joe Maffei, Karl Telleen, Danya Mohr, William Holmes, and Yuki Nakayama. August 2006.
- PEER 2005/08** *Damage Accumulation in Lightly Confined Reinforced Concrete Bridge Columns.* R. Tyler Ranf, Jared M. Nelson, Zach Price, Marc O. Eberhard, and John F. Stanton. April 2006.
- PEER 2005/07** *Experimental and Analytical Studies on the Seismic Response of Freestanding and Anchored Laboratory Equipment.* Dimitrios Konstantinidis and Nicos Makris. January 2005.
- PEER 2005/06** *Global Collapse of Frame Structures under Seismic Excitations.* Luis F. Ibarra and Helmut Krawinkler. September 2005.
- PEER 2005//05** *Performance Characterization of Bench- and Shelf-Mounted Equipment.* Samit Ray Chaudhuri and Tara C. Hutchinson. May 2006.
- PEER 2005/04** *Numerical Modeling of the Nonlinear Cyclic Response of Shallow Foundations.* Chad Harden, Tara Hutchinson, Geoffrey R. Martin, and Bruce L. Kutter. August 2005.
- PEER 2005/03** *A Taxonomy of Building Components for Performance-Based Earthquake Engineering.* Keith A. Porter. September 2005.
- PEER 2005/02** *Fragility Basis for California Highway Overpass Bridge Seismic Decision Making.* Kevin R. Mackie and Božidar Stojadinović. June 2005.

- PEER 2005/01** *Empirical Characterization of Site Conditions on Strong Ground Motion.* Jonathan P. Stewart, Yoojoong Choi, and Robert W. Graves. June 2005.
- PEER 2004/09** *Electrical Substation Equipment Interaction: Experimental Rigid Conductor Studies.* Christopher Stearns and André Filiatrault. February 2005.
- PEER 2004/08** *Seismic Qualification and Fragility Testing of Line Break 550-kV Disconnect Switches.* Shakhzod M. Takhirov, Gregory L. Fenves, and Eric Fujisaki. January 2005.
- PEER 2004/07** *Ground Motions for Earthquake Simulator Qualification of Electrical Substation Equipment.* Shakhzod M. Takhirov, Gregory L. Fenves, Eric Fujisaki, and Don Clyde. January 2005.
- PEER 2004/06** *Performance-Based Regulation and Regulatory Regimes.* Peter J. May and Chris Koski. September 2004.
- PEER 2004/05** *Performance-Based Seismic Design Concepts and Implementation: Proceedings of an International Workshop.* Peter Fajfar and Helmut Krawinkler, editors. September 2004.
- PEER 2004/04** *Seismic Performance of an Instrumented Tilt-up Wall Building.* James C. Anderson and Vitelmo V. Bertero. July 2004.
- PEER 2004/03** *Evaluation and Application of Concrete Tilt-up Assessment Methodologies.* Timothy Graf and James O. Malley. October 2004.
- PEER 2004/02** *Analytical Investigations of New Methods for Reducing Residual Displacements of Reinforced Concrete Bridge Columns.* Junichi Sakai and Stephen A. Mahin. August 2004.
- PEER 2004/01** *Seismic Performance of Masonry Buildings and Design Implications.* Kerri Anne Taeko Tokoro, James C. Anderson, and Vitelmo V. Bertero. February 2004.
- PEER 2003/18** *Performance Models for Flexural Damage in Reinforced Concrete Columns.* Michael Berry and Marc Eberhard. August 2003.
- PEER 2003/17** *Predicting Earthquake Damage in Older Reinforced Concrete Beam-Column Joints.* Catherine Pagni and Laura Lowes. October 2004.
- PEER 2003/16** *Seismic Demands for Performance-Based Design of Bridges.* Kevin Mackie and Božidar Stojadinović. August 2003.
- PEER 2003/15** *Seismic Demands for Nondeteriorating Frame Structures and Their Dependence on Ground Motions.* Ricardo Antonio Medina and Helmut Krawinkler. May 2004.
- PEER 2003/14** *Finite Element Reliability and Sensitivity Methods for Performance-Based Earthquake Engineering.* Terje Haukaas and Armen Der Kiureghian. April 2004.
- PEER 2003/13** *Effects of Connection Hysteretic Degradation on the Seismic Behavior of Steel Moment-Resisting Frames.* Janise E. Rodgers and Stephen A. Mahin. March 2004.
- PEER 2003/12** *Implementation Manual for the Seismic Protection of Laboratory Contents: Format and Case Studies.* William T. Holmes and Mary C. Comerio. October 2003.
- PEER 2003/11** *Fifth U.S.-Japan Workshop on Performance-Based Earthquake Engineering Methodology for Reinforced Concrete Building Structures.* February 2004.
- PEER 2003/10** *A Beam-Column Joint Model for Simulating the Earthquake Response of Reinforced Concrete Frames.* Laura N. Lowes, Nilanjan Mitra, and Arash Altoontash. February 2004.
- PEER 2003/09** *Sequencing Repairs after an Earthquake: An Economic Approach.* Marco Casari and Simon J. Wilkie. April 2004.
- PEER 2003/08** *A Technical Framework for Probability-Based Demand and Capacity Factor Design (DCFD) Seismic Formats.* Fatemeh Jalayer and C. Allin Cornell. November 2003.
- PEER 2003/07** *Uncertainty Specification and Propagation for Loss Estimation Using FOSM Methods.* Jack W. Baker and C. Allin Cornell. September 2003.
- PEER 2003/06** *Performance of Circular Reinforced Concrete Bridge Columns under Bidirectional Earthquake Loading.* Mahmoud M. Hachem, Stephen A. Mahin, and Jack P. Moehle. February 2003.
- PEER 2003/05** *Response Assessment for Building-Specific Loss Estimation.* Eduardo Miranda and Shahram Taghavi. September 2003.
- PEER 2003/04** *Experimental Assessment of Columns with Short Lap Splices Subjected to Cyclic Loads.* Murat Melek, John W. Wallace, and Joel Conte. April 2003.
- PEER 2003/03** *Probabilistic Response Assessment for Building-Specific Loss Estimation.* Eduardo Miranda and Hesameddin Aslani. September 2003.

- PEER 2003/02** *Software Framework for Collaborative Development of Nonlinear Dynamic Analysis Program.* Jun Peng and Kincho H. Law. September 2003.
- PEER 2003/01** *Shake Table Tests and Analytical Studies on the Gravity Load Collapse of Reinforced Concrete Frames.* Kenneth John Elwood and Jack P. Moehle. November 2003.
- PEER 2002/24** *Performance of Beam to Column Bridge Joints Subjected to a Large Velocity Pulse.* Natalie Gibson, André Filiatrault, and Scott A. Ashford. April 2002.
- PEER 2002/23** *Effects of Large Velocity Pulses on Reinforced Concrete Bridge Columns.* Greg L. Orozco and Scott A. Ashford. April 2002.
- PEER 2002/22** *Characterization of Large Velocity Pulses for Laboratory Testing.* Kenneth E. Cox and Scott A. Ashford. April 2002.
- PEER 2002/21** *Fourth U.S.-Japan Workshop on Performance-Based Earthquake Engineering Methodology for Reinforced Concrete Building Structures.* December 2002.
- PEER 2002/20** *Barriers to Adoption and Implementation of PBEE Innovations.* Peter J. May. August 2002.
- PEER 2002/19** *Economic-Engineered Integrated Models for Earthquakes: Socioeconomic Impacts.* Peter Gordon, James E. Moore II, and Harry W. Richardson. July 2002.
- PEER 2002/18** *Assessment of Reinforced Concrete Building Exterior Joints with Substandard Details.* Chris P. Pantelides, Jon Hansen, Justin Nadauld, and Lawrence D. Reaveley. May 2002.
- PEER 2002/17** *Structural Characterization and Seismic Response Analysis of a Highway Overcrossing Equipped with Elastomeric Bearings and Fluid Dampers: A Case Study.* Nicos Makris and Jian Zhang. November 2002.
- PEER 2002/16** *Estimation of Uncertainty in Geotechnical Properties for Performance-Based Earthquake Engineering.* Allen L. Jones, Steven L. Kramer, and Pedro Arduino. December 2002.
- PEER 2002/15** *Seismic Behavior of Bridge Columns Subjected to Various Loading Patterns.* Asadollah Esmaeily-Gh. and Yan Xiao. December 2002.
- PEER 2002/14** *Inelastic Seismic Response of Extended Pile Shaft Supported Bridge Structures.* T.C. Hutchinson, R.W. Boulanger, Y.H. Chai, and I.M. Idriss. December 2002.
- PEER 2002/13** *Probabilistic Models and Fragility Estimates for Bridge Components and Systems.* Paolo Gardoni, Armen Der Kiureghian, and Khalid M. Mosalam. June 2002.
- PEER 2002/12** *Effects of Fault Dip and Slip Rake on Near-Source Ground Motions: Why Chi-Chi Was a Relatively Mild M7.6 Earthquake.* Brad T. Aagaard, John F. Hall, and Thomas H. Heaton. December 2002.
- PEER 2002/11** *Analytical and Experimental Study of Fiber-Reinforced Strip Isolators.* James M. Kelly and Shakhzod M. Takhirov. September 2002.
- PEER 2002/10** *Centrifuge Modeling of Settlement and Lateral Spreading with Comparisons to Numerical Analyses.* Sivapalan Gajan and Bruce L. Kutter. January 2003.
- PEER 2002/09** *Documentation and Analysis of Field Case Histories of Seismic Compression during the 1994 Northridge, California, Earthquake.* Jonathan P. Stewart, Patrick M. Smith, Daniel H. Whang, and Jonathan D. Bray. October 2002.
- PEER 2002/08** *Component Testing, Stability Analysis and Characterization of Buckling-Restrained Unbonded Braces™.* Cameron Black, Nicos Makris, and Ian Aiken. September 2002.
- PEER 2002/07** *Seismic Performance of Pile-Wharf Connections.* Charles W. Roeder, Robert Graff, Jennifer Soderstrom, and Jun Han Yoo. December 2001.
- PEER 2002/06** *The Use of Benefit-Cost Analysis for Evaluation of Performance-Based Earthquake Engineering Decisions.* Richard O. Zerbe and Anthony Falit-Baiamonte. September 2001.
- PEER 2002/05** *Guidelines, Specifications, and Seismic Performance Characterization of Nonstructural Building Components and Equipment.* André Filiatrault, Constantin Christopoulos, and Christopher Stearns. September 2001.
- PEER 2002/04** *Consortium of Organizations for Strong-Motion Observation Systems and the Pacific Earthquake Engineering Research Center Lifelines Program: Invited Workshop on Archiving and Web Dissemination of Geotechnical Data, 4–5 October 2001.* September 2002.
- PEER 2002/03** *Investigation of Sensitivity of Building Loss Estimates to Major Uncertain Variables for the Van Nuys Testbed.* Keith A. Porter, James L. Beck, and Rustem V. Shaikhutdinov. August 2002.
- PEER 2002/02** *The Third U.S.-Japan Workshop on Performance-Based Earthquake Engineering Methodology for Reinforced Concrete Building Structures.* July 2002.

- PEER 2002/01** *Nonstructural Loss Estimation: The UC Berkeley Case Study.* Mary C. Comerio and John C. Stallmeyer. December 2001.
- PEER 2001/16** *Statistics of SDF-System Estimate of Roof Displacement for Pushover Analysis of Buildings.* Anil K. Chopra, Rakesh K. Goel, and Chatpan Chintanapakdee. December 2001.
- PEER 2001/15** *Damage to Bridges during the 2001 Nisqually Earthquake.* R. Tyler Ranf, Marc O. Eberhard, and Michael P. Berry. November 2001.
- PEER 2001/14** *Rocking Response of Equipment Anchored to a Base Foundation.* Nicos Makris and Cameron J. Black. September 2001.
- PEER 2001/13** *Modeling Soil Liquefaction Hazards for Performance-Based Earthquake Engineering.* Steven L. Kramer and Ahmed-W. Elgamal. February 2001.
- PEER 2001/12** *Development of Geotechnical Capabilities in OpenSees.* Boris Jeremić. September 2001.
- PEER 2001/11** *Analytical and Experimental Study of Fiber-Reinforced Elastomeric Isolators.* James M. Kelly and Shakhzod M. Takhirov. September 2001.
- PEER 2001/10** *Amplification Factors for Spectral Acceleration in Active Regions.* Jonathan P. Stewart, Andrew H. Liu, Yoojoong Choi, and Mehmet B. Baturay. December 2001.
- PEER 2001/09** *Ground Motion Evaluation Procedures for Performance-Based Design.* Jonathan P. Stewart, Shyh-Jeng Chiou, Jonathan D. Bray, Robert W. Graves, Paul G. Somerville, and Norman A. Abrahamson. September 2001.
- PEER 2001/08** *Experimental and Computational Evaluation of Reinforced Concrete Bridge Beam-Column Connections for Seismic Performance.* Clay J. Naito, Jack P. Moehle, and Khalid M. Mosalam. November 2001.
- PEER 2001/07** *The Rocking Spectrum and the Shortcomings of Design Guidelines.* Nicos Makris and Dimitrios Konstantinidis. August 2001.
- PEER 2001/06** *Development of an Electrical Substation Equipment Performance Database for Evaluation of Equipment Fragilities.* Thalia Agnanos. April 1999.
- PEER 2001/05** *Stiffness Analysis of Fiber-Reinforced Elastomeric Isolators.* Hsiang-Chuan Tsai and James M. Kelly. May 2001.
- PEER 2001/04** *Organizational and Societal Considerations for Performance-Based Earthquake Engineering.* Peter J. May. April 2001.
- PEER 2001/03** *A Modal Pushover Analysis Procedure to Estimate Seismic Demands for Buildings: Theory and Preliminary Evaluation.* Anil K. Chopra and Rakesh K. Goel. January 2001.
- PEER 2001/02** *Seismic Response Analysis of Highway Overcrossings Including Soil-Structure Interaction.* Jian Zhang and Nicos Makris. March 2001.
- PEER 2001/01** *Experimental Study of Large Seismic Steel Beam-to-Column Connections.* Egor P. Popov and Shakhzod M. Takhirov. November 2000.
- PEER 2000/10** *The Second U.S.-Japan Workshop on Performance-Based Earthquake Engineering Methodology for Reinforced Concrete Building Structures.* March 2000.
- PEER 2000/09** *Structural Engineering Reconnaissance of the August 17, 1999 Earthquake: Kocaeli (Izmit), Turkey.* Halil Sezen, Kenneth J. Elwood, Andrew S. Whittaker, Khalid Mosalam, John J. Wallace, and John F. Stanton. December 2000.
- PEER 2000/08** *Behavior of Reinforced Concrete Bridge Columns Having Varying Aspect Ratios and Varying Lengths of Confinement.* Anthony J. Calderone, Dawn E. Lehman, and Jack P. Moehle. January 2001.
- PEER 2000/07** *Cover-Plate and Flange-Plate Reinforced Steel Moment-Resisting Connections.* Taejin Kim, Andrew S. Whittaker, Amir S. Gilani, Vitelmo V. Bertero, and Shakhzod M. Takhirov. September 2000.
- PEER 2000/06** *Seismic Evaluation and Analysis of 230-kV Disconnect Switches.* Amir S. J. Gilani, Andrew S. Whittaker, Gregory L. Fenves, Chun-Hao Chen, Henry Ho, and Eric Fujisaki. July 2000.
- PEER 2000/05** *Performance-Based Evaluation of Exterior Reinforced Concrete Building Joints for Seismic Excitation.* Chandra Clyde, Chris P. Pantelides, and Lawrence D. Reaveley. July 2000.
- PEER 2000/04** *An Evaluation of Seismic Energy Demand: An Attenuation Approach.* Chung-Che Chou and Chia-Ming Uang. July 1999.
- PEER 2000/03** *Framing Earthquake Retrofitting Decisions: The Case of Hillside Homes in Los Angeles.* Detlof von Winterfeldt, Nels Roselund, and Alicia Kitsuse. March 2000.
- PEER 2000/02** *U.S.-Japan Workshop on the Effects of Near-Field Earthquake Shaking.* Andrew Whittaker, ed. July 2000.

- PEER 2000/01** *Further Studies on Seismic Interaction in Interconnected Electrical Substation Equipment.* Armen Der Kiureghian, Kee-Jeung Hong, and Jerome L. Sackman. November 1999.
- PEER 1999/14** *Seismic Evaluation and Retrofit of 230-kV Porcelain Transformer Bushings.* Amir S. Gilani, Andrew S. Whittaker, Gregory L. Fenves, and Eric Fujisaki. December 1999.
- PEER 1999/13** *Building Vulnerability Studies: Modeling and Evaluation of Tilt-up and Steel Reinforced Concrete Buildings.* John W. Wallace, Jonathan P. Stewart, and Andrew S. Whittaker, editors. December 1999.
- PEER 1999/12** *Rehabilitation of Nonductile RC Frame Building Using Encasement Plates and Energy-Dissipating Devices.* Mehrdad Sasani, Vitelmo V. Bertero, James C. Anderson. December 1999.
- PEER 1999/11** *Performance Evaluation Database for Concrete Bridge Components and Systems under Simulated Seismic Loads.* Yael D. Hose and Frieder Seible. November 1999.
- PEER 1999/10** *U.S.-Japan Workshop on Performance-Based Earthquake Engineering Methodology for Reinforced Concrete Building Structures.* December 1999.
- PEER 1999/09** *Performance Improvement of Long Period Building Structures Subjected to Severe Pulse-Type Ground Motions.* James C. Anderson, Vitelmo V. Bertero, and Raul Bertero. October 1999.
- PEER 1999/08** *Envelopes for Seismic Response Vectors.* Charles Menun and Armen Der Kiureghian. July 1999.
- PEER 1999/07** *Documentation of Strengths and Weaknesses of Current Computer Analysis Methods for Seismic Performance of Reinforced Concrete Members.* William F. Cofer. November 1999.
- PEER 1999/06** *Rocking Response and Overturning of Anchored Equipment under Seismic Excitations.* Nicos Makris and Jian Zhang. November 1999.
- PEER 1999/05** *Seismic Evaluation of 550 kV Porcelain Transformer Bushings.* Amir S. Gilani, Andrew S. Whittaker, Gregory L. Fenves, and Eric Fujisaki. October 1999.
- PEER 1999/04** *Adoption and Enforcement of Earthquake Risk-Reduction Measures.* Peter J. May, Raymond J. Burby, T. Jens Feeley, and Robert Wood.
- PEER 1999/03** *Task 3 Characterization of Site Response General Site Categories.* Adrian Rodriguez-Marek, Jonathan D. Bray, and Norman Abrahamson. February 1999.
- PEER 1999/02** *Capacity-Demand-Diagram Methods for Estimating Seismic Deformation of Inelastic Structures: SDF Systems.* Anil K. Chopra and Rakesh Goel. April 1999.
- PEER 1999/01** *Interaction in Interconnected Electrical Substation Equipment Subjected to Earthquake Ground Motions.* Armen Der Kiureghian, Jerome L. Sackman, and Kee-Jeung Hong. February 1999.
- PEER 1998/08** *Behavior and Failure Analysis of a Multiple-Frame Highway Bridge in the 1994 Northridge Earthquake.* Gregory L. Fenves and Michael Ellery. December 1998.
- PEER 1998/07** *Empirical Evaluation of Inertial Soil-Structure Interaction Effects.* Jonathan P. Stewart, Raymond B. Seed, and Gregory L. Fenves. November 1998.
- PEER 1998/06** *Effect of Damping Mechanisms on the Response of Seismic Isolated Structures.* Nicos Makris and Shih-Po Chang. November 1998.
- PEER 1998/05** *Rocking Response and Overturning of Equipment under Horizontal Pulse-Type Motions.* Nicos Makris and Yiannis Roussos. October 1998.
- PEER 1998/04** *Pacific Earthquake Engineering Research Invitational Workshop Proceedings, May 14–15, 1998: Defining the Links between Planning, Policy Analysis, Economics and Earthquake Engineering.* Mary Comerio and Peter Gordon. September 1998.
- PEER 1998/03** *Repair/Upgrade Procedures for Welded Beam to Column Connections.* James C. Anderson and Xiaojing Duan. May 1998.
- PEER 1998/02** *Seismic Evaluation of 196 kV Porcelain Transformer Bushings.* Amir S. Gilani, Juan W. Chavez, Gregory L. Fenves, and Andrew S. Whittaker. May 1998.
- PEER 1998/01** *Seismic Performance of Well-Confined Concrete Bridge Columns.* Dawn E. Lehman and Jack P. Moehle. December 2000.

## ONLINE REPORTS

The following PEER reports are available by Internet only at [http://peer.berkeley.edu/publications/peer\\_reports.html](http://peer.berkeley.edu/publications/peer_reports.html)

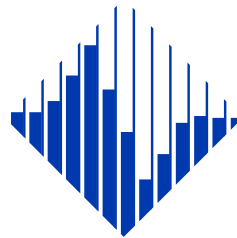
- PEER 2012/102** *Procedure to Restart an Interrupted Hybrid Simulation: Addendum to PEER Report 2010/103.* Vesna Terzic and Božidar Stojadinovic. October 2012.
- PEER 2012/101** *Mechanics of Fiber Reinforced Bearings.* James M. Kelly and Andrea Calabrese. February 2012.
- PEER 2011/107** *Nonlinear Site Response and Seismic Compression at Vertical Array Strongly Shaken by 2007 Niigata-ken Chuetsu-oki Earthquake.* Eric Yee, Jonathan P. Stewart, and Kohji Tokimatsu. December 2011.
- PEER 2011/106** *Self Compacting Hybrid Fiber Reinforced Concrete Composites for Bridge Columns.* Pardeep Kumar, Gabriel Jen, William Trono, Marios Panagiotou, and Claudia Ostertag. September 2011.
- PEER 2011/105** *Stochastic Dynamic Analysis of Bridges Subjected to Spatially Varying Ground Motions.* Katerina Konakli and Armen Der Kiureghian. August 2011.
- PEER 2011/104** *Design and Instrumentation of the 2010 E-Defense Four-Story Reinforced Concrete and Post-Tensioned Concrete Buildings.* Takuya Nagae, Kenichi Tahara, Taizo Matsumori, Hitoshi Shiohara, Toshimi Kabeyasawa, Susumu Kono, Minehiro Nishiyama (Japanese Research Team) and John Wallace, Wassim Ghannoum, Jack Moehle, Richard Sause, Wesley Keller, Zeynep Tuna (U.S. Research Team). June 2011.
- PEER 2011/103** *In-Situ Monitoring of the Force Output of Fluid Dampers: Experimental Investigation.* Dimitrios Konstantinidis, James M. Kelly, and Nicos Makris. April 2011.
- PEER 2011/102** *Ground-motion prediction equations 1964 - 2010.* John Douglas. April 2011.
- PEER 2011/101** *Report of the Eighth Planning Meeting of NEES/E-Defense Collaborative Research on Earthquake Engineering.* Convened by the Hyogo Earthquake Engineering Research Center (NIED), NEES Consortium, Inc. February 2011.
- PEER 2010/111** *Modeling and Acceptance Criteria for Seismic Design and Analysis of Tall Buildings.* Task 7 Report for the Tall Buildings Initiative - Published jointly by the Applied Technology Council. October 2010.
- PEER 2010/110** *Seismic Performance Assessment and Probabilistic Repair Cost Analysis of Precast Concrete Cladding Systems for Multistory Buildings.* Jeffrey P. Hunt and Božidar Stojadinovic. November 2010.
- PEER 2010/109** *Report of the Seventh Joint Planning Meeting of NEES/E-Defense Collaboration on Earthquake Engineering. Held at the E-Defense, Miki, and Shin-Kobe, Japan, September 18–19, 2009.* August 2010.
- PEER 2010/108** *Probabilistic Tsunami Hazard in California.* Hong Kie Thio, Paul Somerville, and Jascha Polet, preparers. October 2010.
- PEER 2010/107** *Performance and Reliability of Exposed Column Base Plate Connections for Steel Moment-Resisting Frames.* Ady Aviram, Božidar Stojadinovic, and Armen Der Kiureghian. August 2010.
- PEER 2010/106** *Verification of Probabilistic Seismic Hazard Analysis Computer Programs.* Patricia Thomas, Ivan Wong, and Norman Abrahamson. May 2010.
- PEER 2010/105** *Structural Engineering Reconnaissance of the April 6, 2009, Abruzzo, Italy, Earthquake, and Lessons Learned.* M. Selim Günay and Khalid M. Mosalam. April 2010.
- PEER 2010/104** *Simulating the Inelastic Seismic Behavior of Steel Braced Frames, Including the Effects of Low-Cycle Fatigue.* Yuli Huang and Stephen A. Mahin. April 2010.
- PEER 2010/103** *Post-Earthquake Traffic Capacity of Modern Bridges in California.* Vesna Terzic and Božidar Stojadinović. March 2010.
- PEER 2010/102** *Analysis of Cumulative Absolute Velocity (CAV) and JMA Instrumental Seismic Intensity ( $I_{JMA}$ ) Using the PEER–NGA Strong Motion Database.* Kenneth W. Campbell and Yousef Bozorgnia. February 2010.
- PEER 2010/101** *Rocking Response of Bridges on Shallow Foundations.* Jose A. Ugalde, Bruce L. Kutter, and Boris Jeremic. April 2010.
- PEER 2009/109** *Simulation and Performance-Based Earthquake Engineering Assessment of Self-Centering Post-Tensioned Concrete Bridge Systems.* Won K. Lee and Sarah L. Billington. December 2009.
- PEER 2009/108** *PEER Lifelines Geotechnical Virtual Data Center.* J. Carl Stepp, Daniel J. Ponti, Loren L. Turner, Jennifer N. Swift, Sean Devlin, Yang Zhu, Jean Benoit, and John Bobbitt. September 2009.

- PEER 2009/107** *Experimental and Computational Evaluation of Current and Innovative In-Span Hinge Details in Reinforced Concrete Box-Girder Bridges: Part 2: Post-Test Analysis and Design Recommendations.* Matias A. Hube and Khalid M. Mosalam. December 2009.
- PEER 2009/106** *Shear Strength Models of Exterior Beam-Column Joints without Transverse Reinforcement.* Sangjoon Park and Khalid M. Mosalam. November 2009.
- PEER 2009/105** *Reduced Uncertainty of Ground Motion Prediction Equations through Bayesian Variance Analysis.* Robb Eric S. Moss. November 2009.
- PEER 2009/104** *Advanced Implementation of Hybrid Simulation.* Andreas H. Schellenberg, Stephen A. Mahin, Gregory L. Fenves. November 2009.
- PEER 2009/103** *Performance Evaluation of Innovative Steel Braced Frames.* T. Y. Yang, Jack P. Moehle, and Božidar Stojadinovic. August 2009.
- PEER 2009/102** *Reinvestigation of Liquefaction and Nonliquefaction Case Histories from the 1976 Tangshan Earthquake.* Robb Eric Moss, Robert E. Kayen, Liyuan Tong, Songyu Liu, Guojun Cai, and Jiaer Wu. August 2009.
- PEER 2009/101** *Report of the First Joint Planning Meeting for the Second Phase of NEES/E-Defense Collaborative Research on Earthquake Engineering.* Stephen A. Mahin et al. July 2009.
- PEER 2008/104** *Experimental and Analytical Study of the Seismic Performance of Retaining Structures.* Linda Al Atik and Nicholas Sitar. January 2009.
- PEER 2008/103** *Experimental and Computational Evaluation of Current and Innovative In-Span Hinge Details in Reinforced Concrete Box-Girder Bridges. Part 1: Experimental Findings and Pre-Test Analysis.* Matias A. Hube and Khalid M. Mosalam. January 2009.
- PEER 2008/102** *Modeling of Unreinforced Masonry Infill Walls Considering In-Plane and Out-of-Plane Interaction.* Stephen Kadysiewski and Khalid M. Mosalam. January 2009.
- PEER 2008/101** *Seismic Performance Objectives for Tall Buildings.* William T. Holmes, Charles Kircher, William Petak, and Nabih Youssef. August 2008.
- PEER 2007/101** *Generalized Hybrid Simulation Framework for Structural Systems Subjected to Seismic Loading.* Tarek Elkhoraibi and Khalid M. Mosalam. July 2007.
- PEER 2007/100** *Seismic Evaluation of Reinforced Concrete Buildings Including Effects of Masonry Infill Walls.* Alidad Hashemi and Khalid M. Mosalam. July 2007.

The Pacific Earthquake Engineering Research Center (PEER) is a multi-institutional research and education center with headquarters at the University of California, Berkeley. Investigators from over 20 universities, several consulting companies, and researchers at various state and federal government agencies contribute to research programs focused on performance-based earthquake engineering.

These research programs aim to identify and reduce the risks from major earthquakes to life safety and to the economy by including research in a wide variety of disciplines including structural and geotechnical engineering, geology/seismology, lifelines, transportation, architecture, economics, risk management, and public policy.

PEER is supported by federal, state, local, and regional agencies, together with industry partners.



PEER Core Institutions:  
University of California, Berkeley (Lead Institution)  
California Institute of Technology  
Oregon State University  
Stanford University  
University of California, Davis  
University of California, Irvine  
University of California, Los Angeles  
University of California, San Diego  
University of Southern California  
University of Washington

PEER reports can be ordered at [http://peer.berkeley.edu/publications/peer\\_reports.html](http://peer.berkeley.edu/publications/peer_reports.html) or by contacting

Pacific Earthquake Engineering Research Center  
University of California, Berkeley  
325 Davis Hall, mail code 1792  
Berkeley, CA 94720-1792  
Tel: 510-642-3437  
Fax: 510-642-1655  
Email: [peer\\_editor@berkeley.edu](mailto:peer_editor@berkeley.edu)

ISSN 1547-0587X